RESEARCH INVESTIGATION RI98-012

STRENGTHENING OF BRIDGE G-270 WITH EXTERNALLY BONDED CARBON FIBER REINFORCED POLYMER (CFRP)

PREPARED FOR THE
MISSOURI DEPARTMENT OF TRANSPORTATION

IN COOPERATION WITH THE
U.S. DEPARTMENT OF TRANSPORTATION
FEDERAL HIGHWAY ADMINISTRATION

Written By:

University of Missouri – Rolla:
Randy Mayo, M. Sc. Candidate
Antonio Nanni, V. & M. Jones Professor
Steve Watkins, Associate Professor

University of Missouri – Columbia:
Michael Barker, Associate Professor

The Pennsylvania State University:
Thomas Boothby, Associate Professor

CENTER FOR INFRASTRUCTURE ENGINEERING STUDIES
UNIVERSITY OF MISSOURI – ROLLA

Submitted
December 1999

The opinions, findings and conclusions expressed in this report are those of the principal investigator and the Missouri Department of Transportation. They are not necessarily those of the U.S. Department of Transportation, Federal Highway Administration. This report does not constitute a standard, specification or regulation

ACKNOWLEDGEMENTS

The Missouri Department of Transportation and the University Transportation Center on Advanced Materials and NDT Technologies at the University of Missouri – Rolla provided financial support.

Master Builders Technologies, Cleveland, OH, provided the CFRP material systems.

Structural Preservation Systems, Baltimore, MD, was the contractor that installed the CFRP systems.

EXECUTIVE SUMMARY

This report presents the results of a pilot study to apply externally bonded Carbon Fiber Reinforced Polymer (CFRP) sheets to strengthen a simple span reinforced concrete solid slab bridge built in 1922. Strengthening with CFRP sheets was accomplished in three days without traffic interruption, and preparation consisted of only light sandblasting. Bridge G-270 is the only load-posted structure on a heavy truck route that serves a lead mining operation and the objective was to strengthen the bridge to allow removal of the load posting. The University of Missouri-Rolla conducted the pilot study for the Missouri Department of Transportation (MoDOT) under MoDOT Contract No. RI98-012.

The laboratory testing included the static flexural test of two full-scale beams, designed as a unit strip from the existing bridge deck, and the fatigue bond test of coupon-type specimens. Two reinforced concrete beams, a control beam and a beam strengthened with externally bonded CFRP were tested under four point bending.

Coupon-type specimens consisting of unreinforced concrete beams with a reversed T-shaped cross-section and with a CFRP sheet applied to the bottom were tested. The purpose was to investigate the behavior of bond between CFRP sheets and concrete under fatigue loading.

The field load testing of the bridge, before and after strengthening, was performed by the University of Missouri-Columbia to verify the performance of the bridge after the application of externally bonded CFRP. Long-term field measurements also were conducted to monitor the durability and the strain condition of the strengthened system. Pennsylvania State University conducted the monitoring of durability by studying the electrochemical effects of the CFRP material on the degradation of the reinforcing steel. Fiber-optic strain sensors were applied to the FRP reinforcement and the concrete to allow for long-term monitoring of the integrity of the FRP reinforcement.

This pilot study was a success. Laboratory and field tests confirmed that CFRP sheets, externally applied to a bridge superstructure, effectively strengthened the slab. Monitoring of the bridge will continue.

TABLE OF CONTENTS

LIST OF ILLUSTRATIONS

LIST OF TABLES

LIST OF SYMBOLS

Symbol		Description
A_1	=	Rating Load Factor applied to M_{ll+i}, 2.17 for Inventory, 1.3 for Operating
A_c	=	Area of concrete gross section (in.^{2})
A_{cr}	=	Area of concrete compression zone after cracking (in.^{2})
A_f	=	Total area of fiber contained in the FRP laminate = $n_p\ t_f\ w_f$ (in.^{2})
$A_{f,est}$	=	Estimated area of carbon fiber (in.^{2})
A_s	=	Area of tension steel (in.^{2})
A'_s	=	Area of compression steel (in.^{2})
b	=	Width of the section (in.)
C	=	Compressive force (lb.)
c	=	Depth to the neutral axis (in.)
c_b	=	Distance from the neutral axis of the gross concrete section to the bonded substrate (in.)
C_D	=	Tensile strength reduction factor for FRP subjected to sustained loading
C_E	=	Tensile strength reduction factor for FRP subjected to environmental conditions
d	=	Depth to the tension steel reinforcement centroid from the extreme compression fiber (in.)
D	=	Density of the material (g/cm^3)
E	=	Electrical potential (mV)
E_c	=	Approximate elastic modulus of concrete in compression (ksi)
E_{corr}	=	Electrical corrosion potential (mV)
E_f	=	Elastic modulus of the FRP fiber material (ksi)
E_s	=	Elastic modulus of reinforcing steel (ksi)
f_c	=	Level of stress in concrete (psi)
f'_c	=	Compressive strength of concrete (psi)
f_f	=	Level of stress in FRP (ksi)
f_{fu}	=	Ultimate stress level of FRP (ksi)
f_r	=	Modulus of rupture of concrete (psi)
f_s	=	Level of stress in steel (psi)
f_y	=	Yield strength of mild steel (psi)
h	=	Total height of the section and depth to the FRP flexural reinforcement (in.)
i	=	Current density (μA/cm^2)
I	=	Live load Impact
i_{corr}	=	Corrosion current (A/cm^2)
I_{cr}	=	Moment of inertia of the cracked concrete section (in.^{4})
I_g	=	Moment of inertia of the gross concrete section (in.^{4})
k	=	Ratio of the depth to the elastic neutral axis to the effective depth, d
LL	=	Live load
$LLDF_{1L}$	=	Live load distribution factor for one lane
$LLDF_{2L}$	=	Live load distribution factor for two lanes
l_n	=	Clear span of the beam (in.)
m	=	Molecular weight (g)
M_{ac}	=	Available capacity for live load moment plus impact (ft-kips)
M_c	=	Moment capacity of concrete based on the allowable stress of concrete controlling. (ft-kips)
M_{cap}	=	Moment capacity (ft-kips)
M_{cr}	=	Cracking moment (ft-kips)
M_{dl}	=	Dead load moment (ft-kips)
M_{ip}	=	Moment due to loads in place at the time of FRP installation. (ft-kips)
M_{ll+i}	=	Live load moment plus impact (ft-kips)
M_n	=	Nominal moment capacity of a section (ft-kips)
M_{serv}	=	Moment due to service loads (ft-kips)
M_s	=	Moment capacity based on the allowable steel stress controlling. (ft-kips)
M_u	=	Moment due to factored loads (ft-kips)
N	=	Number of cycles to failure
n_p	=	Number of fiber plies

n_e = Number of electrons transferred
n_f = Modular ratio of elasticity of fiber reinforcement
n_s = Modular ratio of elasticity of tension steel
P = Static load applied (lbs)
r = Corrosion rate (mm/year)
R_{AS} = Allowable Stress bridge rating
r_g = Radius of gyration of the gross concrete section = $\sqrt{I_g / A_g}$ (in.)
R_{LF} = Load Factor bridge rating
R_p = Polarization resistance (ohms/cm^2)
S = Span length (ft.)
S_f = Ratio between the maximum stress applied during the fatigue loading and the ultimate stress under static loading.
S_m = Section modulus ($in.^3$)
T = Tensile force (lb.)
t_f = Thickness of one ply of fiber sheet (in.)
V = Direct current electrical potential (mV)
V_n = Nominal shear strength (lb.)
V_u = Factored shear (lb.)
w_f = Total width of the FRP laminate (in.)
β_1 = Multiplier on c to determine the depth of an equivalent rectangular stress distribution for concrete
β_a = Anodic Tafel slopes (mV/decade)
β_c = Cathodic Tafel slopes (mV/decade)
ε_b = Strain level in the concrete substrate developed by a given bending moment. Tension is positive. (in/in)
ε_{bi} = Strain level in the concrete substrate at the time of FRP installation. Tension is positive. (in./in.)
ε_c = Maximum compressive strain level in the concrete (in/in)
ε'_c = Strain level in the concrete corresponding to the peak value of stress, f'_c (in./in.)
ε_{cu} = Maximum usable compressive strain in the concrete = 0.003 (in./in.)
ε_f = Strain level in the FRP developed by a given bending moment (in./in.)
ε_{fu} = Ultimate strain (elongation) of the FRP material (in./in.)
ε_s = Strain level in the tension steel (in./in.)
ε_{sy} = Strain level in the tension steel at its yield point = f_y/E_s (in./in.)
ϕ = Strength reduction factor
γ = Multiplier on f'_c to determine the intensity of an equivalent rectangular stress distribution for concrete
ρ = Ratio of tension reinforcement
ρ_b = Reinforcement ratio producing balanced strain conditions

1. INTRODUCTION

1.1. BACKGROUND

The National Research Board (Small, 1998) reports that there are approximately 590,000[1] structures in the National Bridge Inventory database in the United States. Approximately 80 percent (475,850) are classified as bridges with spans 20 feet (6.10 m) or longer. Many of these structures have exceeded their design life and carry loads in excess of their original design. These factors in conjunction with fatigue, deterioration from chlorides used in anti-icing operations, have left many bridges in need of repair, strengthening or replacement.

Of this number, approximately 50,000 are classified as structurally deficient, 89,000 are functionally obsolete and 54,000 are both structurally deficient and functionally obsolete. This means over 40 percent of the nation's bridges need repair or replacement. Due to budget constraints, the cost to repair or replace all of these structures is beyond the financial means of many states. Many states are forced to post load restrictions on their bridges as a stopgap measure until more funds become available for repair or replacement.

The Missouri Department of Transportation (MoDOT) currently has 6,188 bridges on the state highway system, 2,129 of which have restricted load postings.

1.2. SELECTION OF BRIDGE G-270

The bridge selected for demonstration of the CFRP strengthening technology is Bridge G-270 on Route 32 in Iron County (Figure 1.1). A map showing the location of the bridge is presented in Appendix A. The bridge is a 20 foot (6.10 m) solid reinforced concrete (RC) slab built in 1922 with an original roadway width of 18 feet (5.49 m). The bridge currently carries a traffic volume of 1,600 vehicles per day. Around 1990, the original baluster handrails were removed under a construction project, F-32-2(11), and replaced with a thrie-beam guardrail that expanded the roadway width to approximately 20 feet (6.10 m). The bridge has a load restriction posting that limits trucks over 14 tons (124,600 N) to 15 mph (24.14 km/h) on the bridge. The posting also limits truck weights for single axle trucks to 19 tons (169,100 N) and all other trucks to 34 tons (302,600 N) (Figure 1.2). The Missouri Department of Transportation (MoDOT) selected this bridge for evaluation because of its restricted load posting and location near the Doe Run lead mines which generates heavy truck traffic.

1.3. OBJECTIVE

The objective of the project is to increase the flexural capacity of the bridge with the application of externally bonded CFRP.

Verification of the effectiveness of the strengthening system is to be accomplished by laboratory testing of two full-scale beams and in-situ field tests of the actual bridge before and after strengthening. Information on the long-term structural behavior of the strengthened bridge is to be gained by laboratory fatigue testing of coupon-type specimens and by monitoring durability and strain condition of the real structure.

[1] Based on the 1995 National Bridge Inventory Database

Figure 1.1. Bridge G-270

Note: 1 ton = 8,900 N; 1 mile = 1.61 km

Figure 1.2. Load Posting

2. REVIEW OF LITERATURE

2.1. FRP COMPOSITES

Fiber Reinforced Polymer (FRP) material systems, composed of fibers embedded in a polymeric matrix, exhibit several properties which create the opportunity for their use as structural reinforcing elements (Nanni 1993, Nanni and Dolan 1993). They are characterized by excellent tensile strength in the direction of the fibers and by negligible strength in the direction transverse to the fibers. This illustrates the anisotropic nature of these materials. FRP composites do not exhibit yielding, but instead are elastic up to failure. They are also characterized by relatively low modulus of elasticity in tension and low compressive properties. FRP composites are corrosion resistant and should perform better than other construction materials in terms of weathering behavior.

The FRP matrix consists of a polymer, or resin, used as a binder for the reinforcing fibers. The matrix has two main functions. It enables the load to be transferred among fibers and protects the fibers from environmental effects. Three types of commonly available thermo-setting resins are epoxy, vinyl ester and phenolic.

Epoxy resins are the most common and have excellent structural properties as well as excellent adhesion characteristics. Their maximum use temperature is on the order of 200° F (93.3° C). They are used in advanced applications including aircraft, aerospace, and defense as well as many of the first-generation FRP products for concrete currently available in the market. These materials have certain attributes that can be useful in specific circumstances. Epoxy resins are available in a range of viscosities, and will work with a number of curing agents or hardeners. The nature of epoxy allows it to be manipulated into a partially cured or advanced cure state commonly known as a "prepreg". If the “prepreg” also contains the reinforcing fibers, the resulting tacky lamina can be positioned on a mold (or wound if it is in the form of a tape) at room temperature. Epoxy resins are more expensive than commercial polyesters and vinyl esters.

Vinyl ester resins are a lower cost matrix material with good durability characteristics, but have lower structural performance and low resistance to heat.

Phenolic resins are similar to vinyl ester but have a higher resistance to heat and low smoke generation.

Thermo-setting resins are generally heat activated, or cured, from an initial liquid state. Resins are often combined with additives and fillers for environmental resistance, flame retardence, appearance, and cost reduction.

In a composite material, the fibers have the role of the load-bearing constituent. Fibers give the composite high tensile strength and rigidity along their longitudinal direction. Several types of fibers have been developed for use in FRP composites. For structural applications, research and development has been conducted using carbon, aramid and glass fibers. In the order listed, these fibers exhibit an ultimate strain range of 1 to 4%, with no yielding occurring prior to failure. The ultimate strength range is approximately 826,728 to 478,632 psi (5,700 to 3,300 MPa), and elastic moduli range from 39,000 to 10,000 ksi (269 to 69 GPa).

Carbon fibers are the strongest, stiffest, and most durable. There are three sources for commercial carbon fibers: pitch, a by-product of petroleum distillation, PAN (polyacrylonitrile), and rayon. Molecular structure and degree of freedom from defects

control the properties of carbon fiber. The formation of carbon fibers requires processing temperatures above 1830°F (1000°C). At this temperature, most synthetic fibers will melt and vaporize. Acrylic, however, does not, and its molecular structure is retained during high-temperature carbonization. Carbon fibers are not easily wet by resins, particularly in the case of higher-modulus fibers. Surface treatments that increase the number of active chemical groups (and sometimes roughen the fiber surface) have been developed for some resin matrix materials. Carbon fibers are frequently shipped with an epoxy size treatment applied to prevent fiber abrasion, to improve handling, and to provide an epoxy-resin matrix-compatible interface.

Aramid an organic fiber offers excellent impact resistance. It is available in tows, yarns, rovings, and various woven cloth products. These can be further processed to intermediate stages, such as "prepregs".

Glass produces a common, low-cost reinforcing fiber. Glass has been the predominant fiber for many civil engineering applications because of an economical balance of cost and specific strength properties. There are many glass fibers commercially available:

- E-Glass, electrical grade, the most widely used composite reinforcement.
- S2®-Glass, high strength grade.
- ECR-Glass, a modified E-Glass, which provides improved acid resistance.
- AR-Glass, an alkali resistant glass for high alkaline environments.

Glass fibers are very surface-active and are hydrophilic. They can be easily damaged in handling. A protective film former is applied immediately as the first step after the fiber-forming process. Sizing solutions containing the film former also contain an adhesion promoter. Adhesion promoters are usually organo-functional silanes, which function as coupling agents.

Glass fibers are elastic until failure and exhibit negligible creep under controlled dry conditions. Generally, it is agreed that the modulus of elasticity of monofilament E-Glass is approximately 10,600 ksi (73 GPa). The ultimate fracture strain is in the range of 2.5 to 3.5%. The stress-strain characteristics of strands have been thoroughly investigated. When glass fibers are held under a constant load at stresses below the instantaneous static strength, they will fail at some point as long as the stress is maintained above a minimum value. This is called "creep rupture." Atmospheric conditions play a role and water vapor is the most damaging. It has been theorized that the surface of glass contains sub-microscopic voids that act as stress concentrations. Moist air can contain weakly acidic carbon dioxide. The corrosive effect of such exposure can affect the stress in the void regions for glass fiber filaments until failure occurs. In addition, exposure to high pH environments may cause aging or a rupture associated with time.

Composites can be fabricated in a variety of ways. Individual filaments and tows can be wound, pultruded, or laid-up in the final shape. Filament winding entails the wrapping of resin-impregnated (wet or dry) fibers around a mandrel. Pultrusion entails the continuous production of a composite shape by squeezing resin-impregnated fibers through a hot die. Lay-up fabrication consists of the placement of multiple layers of resin-impregnated fibers or fabrics

onto a desired shape. This can be done with pre-impregnated tapes or dry fabrics that are impregnated with resin at the time of lay-up.

FRP composites are used in the construction industry in various forms and systems:

- Sheets of fiber are thin, flexible fabric-like materials. The sheets can either be dry and have the resin applied to them in place, or pre-impregnated "prepreg" with uncured B-stage resin, which requires special storage and handling.
- Laminates are formed from sheets by stacking one or more layers of the sheet and resin to consolidate them into the desired thickness. By adjusting the orientation and stacking sequence of the layers, a variety of physical properties can be achieved.
- Unidirectional sheets having fibers that are all aligned in a common direction.
- Multidirectional sheets are similar to unidirectional sheets except that fibers running in multiple directions are woven together. The fibers used can be of a variety of materials (carbon and aramid, for example) to create hybrid FRP laminates.

FRP composites for externally bonded strengthening can be applied in variety of ways. Resin impregnation may occur before (e.g., pultrusion, "prepreg") or during manufacturing. Pre-impregnated sheets have the advantage of assuring a better "wetting" of the individual fibers, but have disadvantages in terms of shelf life and curing. Individual filaments and tows can be wound, pultruded, braided, or laid up into the final shape. Manual lay-up fabrication that consists of the placement of multiple layers (plies) of resin-impregnated sheets or fabrics onto the concrete surface appears to be particularly promising. Manual lay-up can be done with "prepreg" tapes or dry-fiber sheets to be impregnated at the time of installation. The terms tape and sheet are used interchangeably and indicate a unidirectional product. The term fabric is used to indicate a product where fibers have been arranged in more than one direction. Lay-up of sheets with fibers oriented at different angles allows for the possibility of engineering mechanical properties such as strength and stiffness.

As a point of reference, the thickness of an installed ply (which includes fibers and adhesive) is in range of 0.039 to 0.118 in. (1 to 3 mm). The process followed for the field installation of externally bonded FRP reinforcement consists of the basic following steps: concrete surface preparation (e.g., cleaning, crack sealing, rust-proofing existing steel reinforcement, smoothing, etc.), primer coat application, resin (undercoat) application, adhesion of the sheet(s), resin application, curing, and finish coat application.

Other cured systems include FRP grids (2D and 3D) and FRP reinforcing bars for concrete. High-strength FRP rods can be used for prestressing concrete (either in new construction or in external post-tensioning). Several tendon/anchor systems for concrete prestressing are available worldwide (Nanni 1993).

2.2. EXTERNALLY BONDED REPAIR

Structural retrofit work has come to the forefront of industry practice in response to the problem of aging infrastructure and buildings worldwide. This problem, coupled with revisions in structural codes to better withstand natural phenomena, creates the need for structural retrofit technologies. Some important characteristics of repair work are: labor cost, shut-down costs, material costs, scheduling constraints, long-term durability, difficulty in selection of repair method, and evaluation of effectiveness.

An effective method for upgrading RC members (prestressed and non-prestressed) is plate bonding. This method originates from the strengthening of steel beams by means of adding steel plates. It began in South Africa and France, where steel plates bonded with epoxy resins were used for strengthening of concrete members (L'Hermite and Bresson 1967), and was followed by more than 10 years of research until it became an accepted field practice. Experiments have investigated the influence of factors such as plate thickness, type of adhesive and anchoring conditions (Swamy et al. 1987). Roberts and Haji-Kazemi (1989) published a theoretical study of the behavior of RC beams bonded with steel plates that has become a landmark paper. This study was aimed at developing a simple analytical model capable of predicting the effect of a steel plate on the distribution of strain and stress in the RC beam.

In Germany and Switzerland during the mid 1980's, replacement of steel with FRP plates began to be viewed as a promising improvement in externally bonded repair (Meier 1987, Meier and Kaiser 1991, Rostasy and Budelman 1992). Kaiser (1989) load tested carbon FRP composites and showed the validity of the strain compatibility method (i.e., classical approach for RC sections) in the analysis of repaired members. In the United States Ritchie et al (1991) and Saadatmanesh and Ehsani (1991) studied the static behavior of RC beams with externally bonded glass FRP plates and developed analytical methods also based on strain compatibility. Later, Triantafillou and Plevris (1992) added concepts of fracture mechanics to this classical method. Berset (1992) investigated the use of externally bonded composites to strengthen RC beams in shear. More recently, Plevris and Triantafillou (1994) developed an analytical model for predicting the creep and shrinkage behavior of RC members strengthened with various types of FRP plates. In Saudi Arabia, Sharif et al (1994), using both Roberts' theory and strain compatibility, developed a theoretical algorithm for predicting the flexural strength and the plate separation load of repaired beams.

For bridge structures subjected to cyclic loading, fatigue becomes an important issue that needs to be addressed by the designer. The fatigue behavior of FRP as a stand-alone material has been under investigations for almost 40 years in the context of aerospace, marine and mechanical applications (Broutman, 1974). Over this period of time, fatigue data have been generated for a variety of composite materials under axial and flexural fatigue loading. More recently, research has been carried out on the fatigue behavior of FRP for infrastructure applications (Demers, 1998). In the past decade a remarkable amount of research has focused on the static behavior of RC beams strengthened with externally bonded FRP sheets. However, little has been done on the fatigue performance of RC beams strengthened with externally bonded FRP sheets. The available literature includes papers by Shahawy and Beitelman (1998), Nishizaki et al. (1997) and Demers (1998).

Of all countries, Japan has seen the largest number of field applications using bonded FRP composites. Two large manufacturing industries (Tonen and Mitsubishi Chemical) have aggressively pursued this technology. A joint venture of Mitsubishi Chemical and Obayashi Corporation (a general contractor) was the first partnership to propose and execute column and chimney repair by FRP wrapping. Japanese manufacturer's literature (Tonen 1994, Mitsubishi Chemical 1994) also proposes the adoption of the working stress design method based on the classical flexural theory. The primary assumption remains that of perfect bond between FRP and concrete (and between concrete and steel). Allowable stress for the FRP sheets is set at one-third of the ultimate tensile capacity. This means that the allowable strain in the FRP, even in the case of low-elongation fibers, is larger than five times the strain at yield of conventional Grade 60 steel.

The advantages of FRP versus steel for the reinforcement of concrete structures include lower installation costs, improved corrosion resistance, on-site flexibility of use, and small changes in member size after repair. An additional advantage in terms of industry acceptance is due to the fact that building code enforcement for repair-type application is not as stringent as for new construction.

Implementation of FRP composites as concrete reinforcement in the repair of low-visibility applications such as peripheral beams, balcony parapets, retaining walls, tanks, tunnel linings, and nonstructural walls in buildings could be immediate. Widespread implementation in structural repair is ultimately contingent upon availability of codes and familiarity of owners, engineers, and contractors with the performance of the new materials and technology.

2.3. MONITORING OF DURABILITY

One of the most relevant issues related to the application of FRP composites to strengthen existing structures is their long-term behavior. In the particular case of CFRP, for example, inadvertent electrochemical effects on the degradation of reinforcing steel and vice-versa can occur in a real service environment. The carbon material, very noble by nature, may pose a galvanic corrosion problem in the presence of a less noble material such as reinforcing steel if there is a conductive environment. The effects of the CFRP composite material on steel are still not very clear and, so far, the system (CFRP repair material on RC) seems to work well due to the protective nature of the epoxy matrix material, which acts as a barrier. Until now, there has not been an opportunity for testing the whole system in a real-life application.

In the following, the most commonly used techniques to monitor corrosion of reinforcing steel in concrete are outlined.

2.3.1. Corrosion Potential Measurements. The measurement of the half-cell potential is the most commonly used technique in determining corrosion susceptibility for reinforcing steel in concrete. The potential between the steel and a reference electrode is measured using a high impedance voltmeter (>100 MOhm). Electrical contact is usually made at one point on the steel. The concrete is broken and the reference electrode is pressed up against a wetted sponge. The sponge is placed on a well-wetted concrete surface and the potential difference is measured. Figure 2.1 shows a schematic representation of the potential measurement technique.

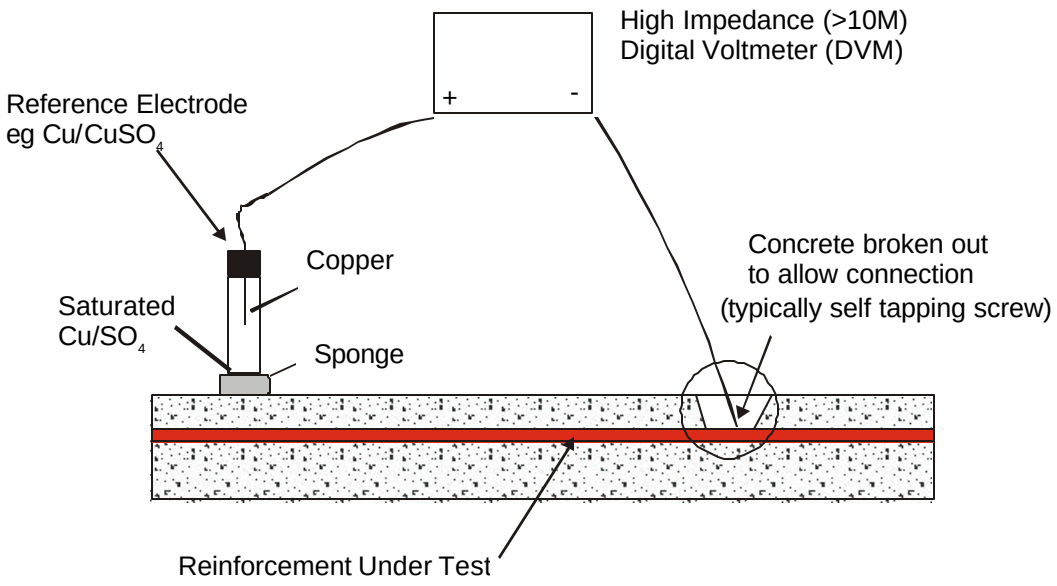

Figure 2.1. Schematic of Half-Cell Potential Measurement Technique

A few important points should be taken into account before any useful data can be obtained. Applying a potential difference across reinforcing steel at different sections of the structure should check the electrical continuity. A measured resistance of less than 1 Ohm is normally considered an indication of a continuous connection of reinforcement. Also, it is important that there is sufficient humidity on the concrete surface so that there is conductivity between the reference electrode and the reinforcing steel.

The ASTM standard describes the following potential values in order to define the active and passive steel conditions:

Potential V(vs. $Cu/CuSO_4$)	***Steel Condition***
> -0.200	Passive
-0.200 to -0.350	Uncertain
<-0.350	Active

It must be noted that these values are given against a copper/copper sulfate electrode. The conversions from one electrode scale to the other can be done by using the following relationships (Jones, 1996), where SHE is the standard hydrogen electrode.

$$V\ (vs.\ SCE) = V\ (vs.\ SHE) - 241\ mV \quad (1)$$

$$V\ (vs.\ CSE) = V\ (vs.\ SHE) - 318\ mV \quad (2)$$

$$V\ (Ag/AgCl) = V\ (vs.\ SHE) - 222\ mV \quad (3)$$

In another study the potential values are given for different types of corrosion of steel in concrete (Wheat and Eliezer, 1985):

State	***Potential mV (SCE)***
Passive (No chloride)	+200 to -600

Passive (in aerated concrete)	+100 to -200
Pitting	-200 to -500
General Corrosion	-450 to -600
Active (limited access O_2)	-1000

2.3.2. <u>Polarization Resistance.</u> The polarization resistance method utilizes a potentiostat to sweep a small range DC potential (at a low scan rate like 0.1 mV/s) around the open circuit potential condition while the current response is recorded. Usually the potential sweep starts at a value 20 mV below open circuit potential and stops 20 mV above the open circuit potential, for total range of 40 mV (Berke and Hicks, 1990).

Over this potential range, the current vs. voltage curve is roughly linear. From this linear relationship it is possible to estimate polarization resistance, R_p, which is used to calculate the corrosion current, i_{corr}, and corrosion rate via following equations:

$$R_p = \frac{dE}{di} = \left.\frac{\Delta E}{\Delta i}\right|_{E=E_{corr}} \tag{4}$$

$$i_{corr} = \frac{1}{R_p}\frac{b_a b_c}{2.3(b_a + b_c)} \tag{5}$$

$$r = 0.00327\frac{m i_{corr}}{n_e D} \tag{6}$$

Where β_a, β_c are anodic and cathodic Tafel slopes, m is the molecular weight of the material (g), n_e is the number of electrons transferred, D is the density of the material (g/cm^3), i is the current density (μA/cm^2) and r is the corrosion rate (mm/year) (Shaw et al., 1997).

The Tafel constants depend upon the resistivity of concrete, and are determined from Tafel plot experiments. The constants are usually in the range of 400 to 500 mV/decade for anodic branch and 250 to 350 mV/decade for the cathodic branch (Al-Tayyib and Khan, 1988). Based on the results from laboratory, outdoor exposure site, and field tests, certain guidelines are available in the literature. A summary of this data is presented below (Clear, 1990).

i_{corr} (mA/ft^2) value	***Damage***
<0.2	no corrosion damage expected
0.2 to 1.0	corrosion damage possible in the range of 10 to 15 years
1.0 to 10	corrosion damage expected in 2 to 10 years
>10	corrosion damage is expected in 2 years or fewer

Reliable and reproducible values of polarization resistance can be obtained only after achieving good electrical contact (via appropriate wetting with water or the use of conductive paste) between the concrete surface and reinforcing steel. That is where a major problem arises: the resistance of concrete. The resistance of the concrete can be on the order of several kOhm/cm^2, which would highly affect the measurements. Therefore, the resistance of the

concrete should be known in order to calculate true polarization resistance. This problem can be overcome by using the "IR compensation" feature present on most commercial potentiostats, or the concrete resistance can be measured using another technique such as EIS.

2.3.3 <u>Electrochemical Impedance Spectroscopy (EIS).</u> EIS is thought to be an excellent tool for monitoring the corrosion of reinforcing steel in concrete since the technique is independent of resistivity of the medium. As was mentioned previously, the EIS data usually requires some interpretation. Potential data and impedance curves representing different stages of corrosion process of reinforcing steel in concrete are summarized and presented in Figure 2.2. In short, the corrosion process can be explained in three stages.

- In the initial stage the steel surface in a passive state gives a noble potential being a part of the large semi-circle of the impedance curve.
- In the second stage the passive film is broken by Cl^- ions and corrosion is initiated, leading to less noble potential. This phenomenon gives two types of impedance curve depending on the wetness of the concrete. Namely in dry condition, where O_2 diffusion into concrete is accelerated, the impedance curve shows a semi-circle. In wet condition the curve shows two separate semi-circles with the corrosion rate determined by the O_2 diffusion process.
- In the third stage corrosion develops around steel surfaces, giving a comparably noble potential and a small imperfect semi-circle in the impedance curve (Andrade et al, 1986).

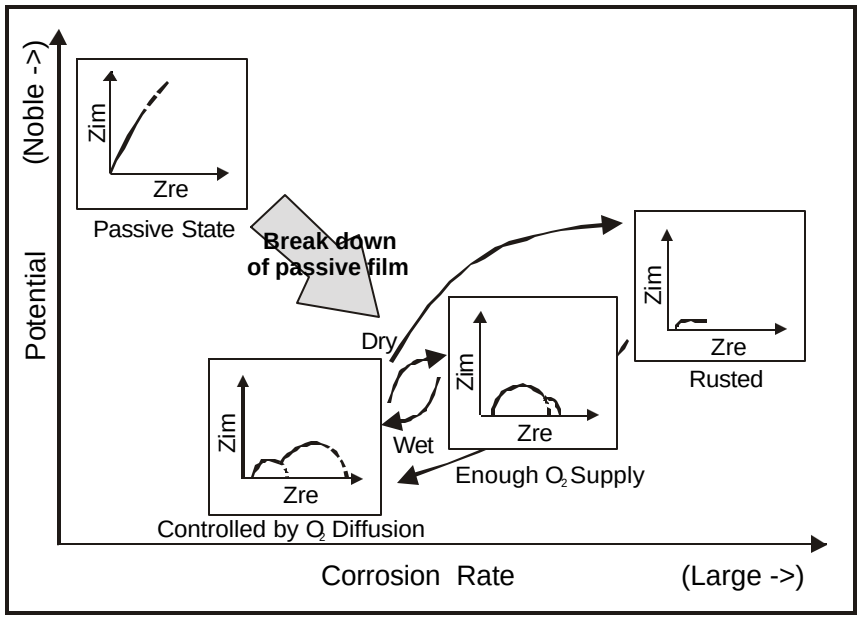

Figure 2.2. Schematic Illustration of Corrosion Data Obtained Using Potential and Impedance Curves.

Different Nyquist and Bode plots obtained when steel is embedded in concrete are presented in Figure 2.3. For example in Figure 2.3a, the reinforcing bars were embedded in mortar without admixtures. In Figure 2.3b calcium chloride was added to the mortar and the steel was attacked by pitting. In Figure 2.3c the mortar was carbonated, thus the whole surface of the steel was uniformly corroding. The analysis of data usually requires knowledge of an equivalent

circuit. In the past, researchers proposed various equivalent circuits for corrosion of reinforcing steel in concrete. Every model tries to take into account the resistive and dielectric properties of the concrete cover, and the resistive and dielectric properties of the lime layer. Unfortunately, the corrosion of steel in concrete is not so simple because the system has a very high resistance, frequently has a passive film, and often corrosion is controlled by diffusion. The most difficult issue in determining the corrosion rate of steel in concrete is that one cannot determine the true values of the electrochemical parameters such as the polarization resistance and the impedance at each position to be measured. The degree of polarization of the reinforcing steel surface, induced by the over-potential applied at corrosion potential, gradually decreases with the distance from the counter electrode (Matsuoka et al., 1990).

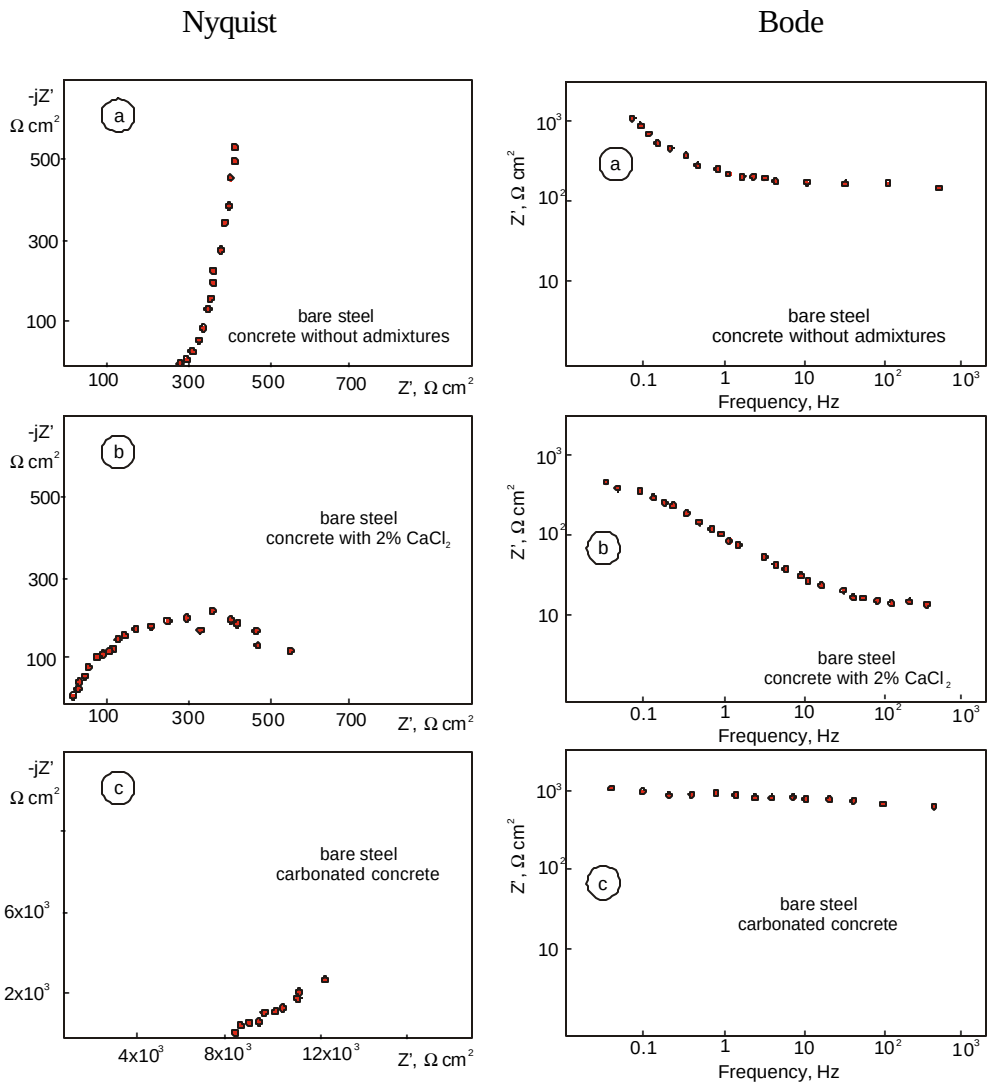

Figure 2.3. Nyquist and Bode Plots of Steel Bars Embedded in Mortar.

2.4. APPLICATIONS

Recently completed strengthening projects (Nanni 1997) are presented herein to demonstrate that CFRP is becoming an acceptable rehabilitation method for buildings and infrastructures. The presented projects show the adaptability of CFRP technology to different situations: correction of design/construction errors and loss of integrity due to vehicular collision. As the technology matures, a field of application that is equally viable and important is that of damage prevention.

2.4.1. Highway Application. Figure 2.4 shows the effect of a vehicular impact on the four girders of the bridge overpass on highway Appia near Terracina, Rome (Nanni 1997). This is a short bridge, 34.48 ft (10.5 m) in span, made of four prestressed concrete girders having cross sectional dimensions of 3.28 by 4.92 ft (1.0 by 1.5 m). The conventional reinforcement (prestressing tendons and reinforcing bars) is clearly visible in the photograph after the loose concrete was removed.

Figure 2.4. Girder Damage Due to Vehicular Impact

The concrete cross section was restored with no-shrink mortar and, after surface preparation, CFRP sheets were adhered as shown in Figure 2.5. The objective of the CFRP strengthening was to make up for the loss of prestress. For each beam, three sheets, 1.08 ft (0.33 m) wide and 9.84 ft (3.0 m) long, were bonded to the soffit (0º fiber direction), and four strips, 0.52 ft (0.16 m) wide and 9.84 ft (3.0 m) long, were wrapped around the three sides (90º fiber direction). The total amount of CFRP material used was approximately 215.27 ft^2 (20 m^2).

Figure 2.5. Pattern of CFRP Strips

The repair of the short columns that transfer load from the RC deck to the RC arch in the viaduct along historical "Via Flaminia", near Spoleto, underwent rehabilitation during the summer of 1996. The bridge was built immediately after World War II. Figure 2.6 shows a snapshot of the bridge, where the row of the shortest columns visible in the center of the photograph represents the area of interest. These columns have a cross-section of 15.7 by 15.7 in. (0.4 by 0.4 m), and are 5.4 ft (1.65 m) tall. Figure 2.7 offers a detailed image of the short columns and their level of deterioration. Concrete had spalled off due to steel reinforcement corrosion. After removal of all deteriorated materials, the original cross section was restored with non-shrinkage mortar and the steel reinforcement was protected with a passivating coat. Finally, the columns were wrapped with a single ply of CFRP sheets as shown in Figure 2.8.

The reinforcement configuration of this column is such that column ends act as hinges, therefore the CFRP wrapping with transverse fibers only is an ideal medium to provide confinement without adding any bending stiffness or moment capacity at the location of the hinges.

Figure 2.6. View of Bridge

Figure 2.7. Deteriorated Columns

Figure 2.8. Application of the CFRP to Column

2.4.2. Building Application. The post-tensioned PC slab of a parking garage in Atlanta, Georgia was strengthened with gunite RC beams shortly after construction in order to correct a deficiency in the number of steel tendons along the East-West alignment of the building. These beams were 0.246 ft (75 mm) deep, 3.28 ft (1 m) wide and reinforced with 6-#9 (28.7 mm diameter) bars. The beams were 17.06 ft (5.2 m) long and ran along the column line, connecting the column capitals 9.84 by 9.84 ft (3 by 3 m). The integrity of the composite action between gunite beam and slab was to be based solely on the strength of the interfacial bond between the two. Since delamination had occurred over time, such action was compromised and epoxy injection was required. In order to find a permanent solution to the problem, it was suggested that the gunite beams be demolished and replaced with two double-ply strips of CFRP.

Figure 2.9 shows the application of the second ply for one of the strips. The two CFRP strips were located at the side of the demolished gunite beam so that adhesion would take place on a relatively smoother concrete surface.

In order to evaluate the condition of the PC slab with and without the gunite beams and also after strengthening with CFRP, a number of rapid load tests were carried out. In the test set-up, a concentrated force was applied to the slab column-strip by means of hydraulic jacks (Figure 2.10). As seen in the photograph, the jacks are reacting against the floor above, which in turn is shored for additional safety. This configuration may be defined as a "push-type" test where the dead weight of the two floors above provides the counterweight. Deflection at several points (e.g., under the load, at the quarter-span sections, at the drop panel) was measured (Figure 2.11). Following repeated loading-unloading cycles, it is possible to develop a hysteresis diagram for the slab. First, the level of the maximum load was calibrated based on preliminary calculations and the response of the structure during test. Second, the load test was repeated with the same modality after the execution of the CFRP strengthening work. Then finally the maximum load was then applied to simulate service conditions. By comparing the outcome of the various tests, it was shown that the CFRP repair was comparable in strength to the gunite beams. CFRP should provide a permanent solution.

Figure 2.9. Application of CFRP Sheet

Figure 2.10. Site Load Test of the Repaired Structure

Figure 2.11. Measurement of Deflection During Loading

3. BRIDGE RATING

3.1. GENERAL REQUIREMENTS

An accurate rating of the existing bridge live load capacity is the first step in determining the need for strengthening. The evaluation included review of the bridge construction drawings, visual inspection, and use of established state and federal guidelines (AASHTO, 1996).

Until recently, MoDOT used two rating methods, the Load Factor Method or the Allowable Stress Method, to rate all their bridges. According to MoDOT's current load rating guidelines, any structure built, rehabilitated, or reevaluated shall be rated using the Load Factor rating Equation (7).

$$R_{LF} = \frac{M_{cap} - 1.3M_{dl}}{A_1 M_{ll+i}} \tag{7}$$

The current load posting on Bridge G-270 was developed using the Allowable Stress rating Equation (8)

$$R_{AS} = \frac{M_{cap} - M_{dl}}{M_{ll+i}} \tag{8}$$

All bridges should be rated at two load levels, the maximum load level called the Operating Rating and a lower load level called the Inventory Rating. The Operating Rating is the maximum permissible load that should be allowed on the bridge. Exceeding this level could damage the bridge. The Inventory Rating is the load level the bridge can carry on a daily basis without damaging the bridge.

In Missouri, the Inventory Rating and Operating Rating, for the Allowable Stress Method, are established at the 55% and 75% stress levels in the reinforcement, respectively. For the Load Factor Method the Operating Rating is based upon the appropriate ultimate capacity using current AASHTO specifications. The Inventory Rating is taken as 60% of the Operating Rating.

The vehicle used for the live load calculations in both the Allowable Stress Method and the Load Factor Method is the HS20 truck or MS18 truck if a metricload rating is desired. If these stress levels are exceeded, load posting may be required.

In Missouri, load posting is established using the H20 and 3S2 vehicles at the 68% stress level for the Allowable Stress Method or at 86% of the Operating Rating for the Load Factor Method. Additionally, the Operating Rating is calculated for the MO-5, HS20 and the 4S3P vehicles. The legal load in Missouri is 23 tons (204,700 N) for H20 vehicles and 40 tons (356,000 N) for 3S2 vehicles. See Appendix D for typical axle loads and spacing for the various rating vehicles.

3.1.1. Live Load Distribution Factors. The two-lane live load distribution width is determined from the AASHTO Standard Specifications for Highway Bridges (AASHTO, 1996) and is shown in Equation (9) with S being the span length in feet.

$$LLDF_{2L} = 4 + 0.06(S) \leq 7.0' \tag{9}$$

Substituting the center to center of support distance of 21.25 feet (6.48 m) for S

$$LLDF_{2L} = 4 + 0.06(21.25) = 5.275 \tag{10}$$

then taking the reciprocal of the live load distribution factor converts the factor for a unit strip.

$$1/LLDF_{2L} = 1/5.275 = 0.1896 \tag{11}$$

MoDOT's live load distribution factor for one-lane loading on slab-type structures, Equation (12), is calculated by assuming the distribution of two wheel loads over the roadway width not to exceed 24 feet (7.32 m).

$$LLDF_{1L} = \frac{2\ Wheel\ Lines}{Roadway\ Width} \tag{12}$$

Substituting 18 feet (5.49 m) for the roadway width will result in the one-lane distribution factor.

$$LLDF_{1L} = \frac{2}{18} = 0.1111 \tag{13}$$

3.1.2. Allowable Stress Rating. Using the Allowable Stress Method, moments and stresses in the concrete and reinforcing steel may be determined by Equations (14) through (16).

$$\tfrac{1}{2} f_c kd\, b = A_s f_s \tag{14}$$

$$M_c = \tfrac{1}{2} f_c kd\, b\left(d - kd/3\right) \tag{15}$$

$$M_s = A_s f_s \left(d - kd/3\right) \tag{16}$$

For the section shown in Figure 3.1 to be in equilibrium, the summation of horizontal forces must equal zero and the summation of moments must equal zero.

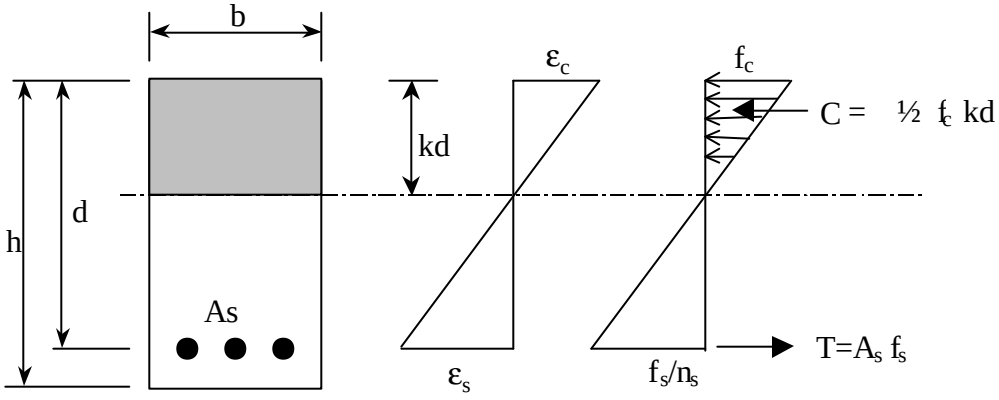

Figure 3.1. Strain and Stress Diagrams for Working Stress

$$T = C \tag{17}$$

$$A_s f_s = \tfrac{1}{2} f_c kdb \tag{18}$$

$$f_c = \frac{f_s / n_s}{d - kd} kd \tag{19}$$

By substituting Equation (19) into Equation (18) and rearranging the terms into a quadratic equation.

$$\frac{b(kd)^2}{2} + n_s A_s (kd) - n_s A_s d = 0 \tag{20}$$

Based on the values in Table 3.1 and substituting into Equation (20)

Table 3.1. Slab Unit Strip Properties

b (in.)	h (in.)	d (in.)	As ($in.^2$)	Ec (ksi)	f'c (psi)	n_s	Es (ksi)	fy (psi)
12	18.5	16.75	1.53	2,770	2363	10	29,000	30,000

Note: 1 ksi = 1,000 psi = 6.89 MPa; 1 in. = 25.4 mm

$$\frac{12(kd)^2}{2} + (10)(1.53)kd - (10)(1.53)(16.75) = 0 \tag{21}$$

Solving the Equation (21) for kd

kd = 5.38" (13.66 cm)

and substituting into Equations (15) and (16) using AASHTO guidelines where f_c equals $0.4f'_c$ or 945 psi (6.52 MPa) and f_s equals $0.55f_y$ or 16,500 psi (113.7 MPa) determines the controlling moment capacity based on the concrete or reinforcing steel allowable stress respectively.

$$M_c = \tfrac{1}{2}(945)(5.38)(12)\left(16.75 - 5.38/3\right) / 12000 = 38.0 \text{ ft} \cdot \text{kips} \ (51.5 \text{ kN-m}) \tag{22}$$

$$M_s = (1.53)(16500)\left(16.75 - 5.38/3\right)/12000 = 31.5 \text{ ft} \cdot \text{kips} \ (42.7 \text{ kN-m}) \tag{23}$$

Continuing this process yields the values shown in Table 3.2 for the various stress levels allowed for Operating, Inventory, and Posting loadings. The moment capacity of the slab is limited by the moment capacity of the reinforcement, therefore the slab is under-reinforced.

Table 3.2. Total Moment Capacity/Foot Width

TRUCK	STRESS LEVEL%-TYPE (Based upon steel stress)	STEEL	CONCRETE	CONCRETE	STEEL
		f_s	f_c	M_c	M_s
		psi	psi	ft-kips	ft-kips
HS20	(55%)-Inventory	16500	945	38.0	31.5
MO5	(75%)-Operating	22500	1289	51.9	42.9
HS20	(75%)-Operating	22500	1289	51.9	42.9
4S3P	(75%)-Operating	22500	1289	51.9	42.9
3S2	(68%)-Posting	20400	1169	47.0	38.9
H20	(68%)-Posting	20400	1169	47.0	38.9

Note: 1 ft-kip = 1,000 ft-lbs = 1.356 kN-m; 1000 psi = 6.89 MPa

Dead load moments due to member self-weight and superimposed loads are tabulated in Table 3.3. This includes the weight of the thrie-beam rail, concrete curb, 7 inch (17.78 cm) asphalt wearing surface and 9.5 inches (24.13 cm) of soil between the wearing surface and the bridge slab. See Appendix B for bridge slab details.

Table 3.3. Service Dead Load Moments/Foot Width

DEAD LOAD	M_{dl}
	ft-kips
MEMBER WEIGHT	13.1
SUPERIMPOSED	9.6
TOTAL	22.6

Note: 1 ft-kip = 1.356 kN-m

The moment capacity available for live load plus 30% impact is the subtraction of the dead load moments from the total moment capacity and is listed in Table 3.4.

Table 3.4. Available Capacity for LL+I/Foot Width

TRUCK	STRESS LEVEL%-TYPE (Based upon steel stress)	M_{ac}
		ft-kips
HS20	(55%)-Inventory	8.8
MO5	(75%)-Operating	20.3
HS20	(75%)-Operating	20.3
4S3P	(75%)-Operating	20.3
3S2	(68%)-Posting	16.3
H20	(68%)-Posting	16.3

Note: 1 ft-kip = 1.356 kN-m

The maximum live load moment for the standard vehicles is calculated using the influence line for moment at center span. The maximum live load moments for the standard trucks are shown in Table 3.5.

Table 3.5. Two Lane Live Load Moments/Foot Width

TRUCK LOADING			
TRUCK	STRESS LEVEL%-TYPE (Based upon steel stress)	M_{ll+i}	LOCATION 1st WHEEL
		ft-kips	ft.
HS20	(55%)-Inventory	20.9	-3.375
MO5	(75%)-Operating	23.9	-28.583
HS20	(75%)-Operating	20.9	-3.375
4S3P	(75%)-Operating	29.0	-8.545
3S2	(68%)-Posting	17.2	-1.375
H20	(68%)-Posting	17.2	-1.479

Note: 1 ft-kip = 1.356 kN-m; 1 ft.= 0.3048 m

The final rating is determined by using Equation (8). The Allowable Stress ratings are tabulated in Table 3.6.

Table 3.6. Allowable Stress Bridge Rating

TWO LANE SAFE LOAD CAPACITY			
TRUCK	FACTOR	TONS	TYPE
HS20	0.422	15.2	Inventory
MO5	0.847	31.0	Operating
HS20	0.968	34.8	Operating
4S3P	0.699	41.9	Operating
3S2	0.945	34.6	Posting
H20	0.945	18.9	Posting

Note: 1 ton = 8.9 kN

In order to remove the posting the 2-lane safe load capacity at the 68 percent operating stress level must be 23 tons (204,700 N) for the H20 vehicle and 40 tons (356,000 N) for the 3S2 vehicle. The required moment capacity to carry the desired loads is shown in Equation (24).

$$\text{Required Moment Capacity} = \frac{\text{Capacity (tons)}}{\text{Vehicle Weight (tons)}}\left(M_{ll+i}\right) + M_{dl} \qquad (24)$$

For the H20 vehicle the moment capacity required is

$$\frac{23}{20}(17.2)+22.6=42.38\approx 42\ \text{ft}\cdot\text{kips}\ (56.95\ \text{kN}\cdot\text{m}) \tag{25}$$

which evaluates to a 8.9 percent increase required in moment capacity. Checking the capacity required for the 3S2 vehicle evaluates to a 6.4 percent increase required in moment capacity. Therefore, the H20 vehicle determines the increase in strength required using the Allowable Stress Rating.

3.1.3. <u>Load Factor Rating.</u> Using the Ultimate Strength Method, the moment capacity may be determined by Equations (26) and (27). Equation (26) is based on the assumption that $\varepsilon_s > \varepsilon_{sy}$, which can be verified if $\rho < \rho_b$ by using Equation (28)**.**

$$M_n = A_s f_y\left(d-\frac{b_1 c}{2}\right) \tag{26}$$

$$M_u \le f M_n \tag{27}$$

$$r_b = 0.85 b_1 \frac{f_c'}{f_y}\left(\frac{87000}{87000+f_y}\right) \tag{28}$$

Based on the slab unit strip property values in Table 3.7 and substituting into Equations (28) and (30).

Table 3.7. Slab Unit Strip Properties

b (in.)	h (in.)	d (in.)	As ($in.^2$)	Ec (ksi)	f'c (psi)	β_1	γ	Es (ksi)	fy (psi)
12	18.5	16.75	1.53	2,770	2363	0.85	0.85	29,000	30,000

Note: 1 ksi = 6.89 MPa; 1 in. = 25.4 mm

$$r_b = 0.85(0.85)\frac{2363}{30000}\left(\frac{87000}{87000+30000}\right)=0.0423 \tag{29}$$

$$r=\frac{A_s}{bd} \tag{30}$$

$$r=\frac{1.53}{(12)(16.75)}=0.0076 \tag{31}$$

Therefore, Equation (26) is valid and can be utilized to determine the moment capacity of a unit strip of bridge slab.

For the section shown in Figure 3.2 to be in equilibrium, the summation of horizontal forces must be equal as shown in Equation (32).

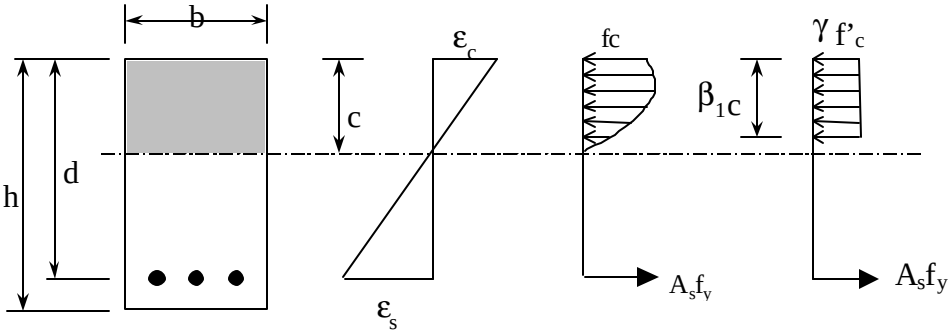

Figure 3.2. Strain and Stress Diagrams for Load Factor

$$g\ f_c' b b_1 c = A_s f_y \tag{32}$$

Based on the values in Table 3.7 and substituting into Equation (32),

$$(0.85)(2363)(12)(0.85)c = (1.53)(30{,}000) \tag{33}$$

Solving the equation for *c*,

$$c = 2.24\text{”}\ (5.69\ \text{cm})$$

and substituting into Equations (26) and (27) determines the moment capacity.

$$M_n = (1.53)(30000)\left(16.75 - \frac{(0.85)(2.24)}{2}\right)/12000 = 60.43\ \text{ft}\cdot\text{kips}\ (81.94\ \text{kN}\cdot\text{m}) \tag{34}$$

$$M_u \le f\ M_n = (0.9)(60.43) = 54.4\ \text{ft}\cdot\text{kips}\ (73.77\ \text{kN}\cdot\text{m}) \tag{35}$$

Continuing this process yields the values shown in Table 3.8 for the various stress levels required for Operating and Inventory loadings.

Table 3.8. Ultimate Capacities/Foot Width

TRUCK	STEEL	CONCRETE	CAPACITY
	f_y	f'_c	ϕM_n
	psi	psi	ft-kips
HS20	30000	2363	54.4
MO-5	30000	2363	54.4
HS20	30000	2363	54.4
4S3P	30000	2363	54.4
3S2	30000	2363	54.4
H20	30000	2363	54.4

Note: 1 ksi = 6.89 MPa; 1 ft-kip = 1.356 kN-m

Dead load moments due to member self-weight and superimposed loads are tabulated in Table 3.9. This includes the weight of the thrie-beam rail, curb, 7 inch (17.78 cm) asphalt wearing surface and the soil between the wearing surface and the bridge slab. See Appendix B for bridge slab details.

Table 3.9. Service Dead Load Moments/Foot Width

DEAD LOAD	M_{dl}
	ft-kips
MEMBER WEIGHT	13.1
SUPERIMPOSED	9.6
TOTAL	22.6

Note: 1 ft-kip = 1.356 kN-m

The moment capacity available for the factored live load plus 30% impact, as listed in Table 3.10, is the subtraction of factored dead load moments from the total moment capacity and divided by the appropriate Rating Load Factor (A_1).

Table 3.10. Available Capacity for LL+I/Foot Width

TRUCK	RATING TYPE	M_{ac}
		ft-kips
HS20	Inventory	11.5
MO5	Operating	19.2
HS20	Operating	19.2
4S3P	Operating	19.2
3S2	Posting	16.5
H20	Posting	16.5

Note: 1 ft-kip = 1.356 kN-m

The maximum live load moment for the standard vehicles is calculated using the influence line for moment at center span. The maximum live load moments for the standard trucks are shown in Table 3.11.

Table 3.11. Two Lane Live Load Calculations/Foot Width

TRUCK LOADING			
TRUCK	RATING TYPE	M_{ll+i}	LOCATION 1st WHEEL
		ft-kips	ft.
HS20	Inventory	20.9	-3.375
MO5	Operating	23.9	-28.583
HS20	Operating	20.9	-3.375
4S3P	Operating	29.0	-8.545
3S2	Posting	17.2	-1.375
H20	Posting	17.2	-1.479

Note: 1 ft-kip = 1.356 kN-m; 1 ft.= 0.3048 m

The final rating is determined by using Equation (7). The Load Factor ratings are tabulated in Table 3.12.

Table 3.12. Load Factor Bridge Rating

TWO LANE SAFE LOAD CAPACITY			
TRUCK	FACTOR	TONS	TYPE
HS20	0.550	19.8	Inventory
MO5	0.803	29.4	Operating
HS20	0.919	33.1	Operating
4S3P	0.662	39.7	Operating
3S2	0.959	35.1	Posting
H20	0.959	19.2	Posting

Note: 1 ton = 8.9 kN

In order to remove the posting the 2-lane safe load capacity at 86 percent of the operating level must be 23 tons (204,700 N) for the H20 vehicle and 40 tons (356,000 N) for the 3S2 vehicle. The required moment capacity to carry the desired loads is shown in Equation (36).

$$\text{Required Moment Capacity} = \frac{\text{Capacity (tons)}}{(0.86)\,\text{Vehicle Weight (tons)}}\left((1.3)M_{ll+i}\right)+(1.3)M_{dl} \tag{36}$$

For the H20 vehicle the moment capacity required is

$$\frac{23}{(0.86)20}(1.3)(17.2)+(1.3)22.6=59.28\approx 60\ \text{ft}\cdot\text{kips}\ (81.36\ \text{kN}\cdot\text{m}) \tag{37}$$

which evaluates to a 9.0 percent increase required in moment capacity. Checking the capacity required for the 3S2 vehicle evaluates to a 6.2 percent increase required in moment capacity. Therefore, the H20 vehicle determines the increase in strength required using the Load Factor Rating.

4. CFRP DESIGN CALCULATIONS

4.1. EXISTING CONDITIONS

The rating calculations show that Bridge G-270 requires strengthening in order to carry current traffic loads. Based on the bridge rating analysis, the new service loads will produce a maximum positive bending moment of M_{serv} = 42 kip·ft/ft (186.9 kN·m/m), and the total factored loads result in a design moment of M_u = 60 kip·ft/ft (267.0 kN·m/m). Material properties established by MoDOT result in a nominal concrete strength f'_c = 2,363 psi (16,292 kPa) and a yield strength for the mild steel of f_y = 30,000 psi (206,843 kPa). However, these bending moments are based on "as built" plans assuming no section losses. From field observations it was evident that some concrete deterioration and reinforcement corrosion has taken place. From past experience bridge decks of this age with an asphalt overlay experience 1 to 2 inches (2.54 to 5.08 cm) of concrete deterioration. This deteriorated concrete is located at the interface of the concrete deck and the asphalt wearing surface. This reduction in effective depth will result in an additional 6 to 9 percent loss in moment capacity. Figure 4.1. shows the dimensions of the one foot wide cross-section adopted in the analysis that follows.

Note: 1 in = 2.54 cm

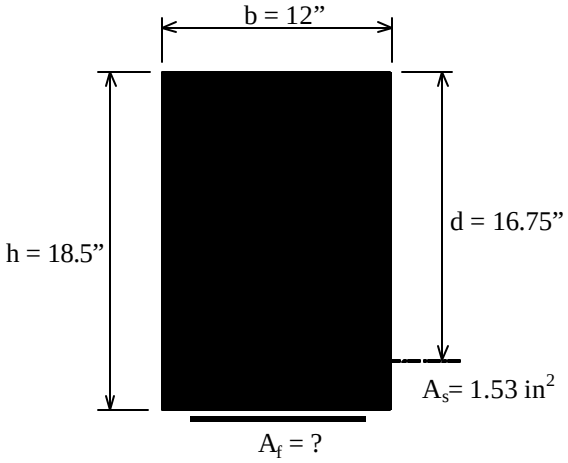

Figure 0.1. Dimensions of the Cross-section

4.1.1. Initial Strains. Based on existing conditions, the total moment in place at the time that the FRP is installed is the dead load moment M_{ip} = 22.6 ft-kip (30.6 kN-m). The strain may be computed for this moment assuming the section is cracked by using Equation (41).

$$M_{cr} = f_r S_m \tag{38}$$

$$M_{cr} = 7.5\sqrt{f'_c}\,\frac{I_g}{h/2} = 7.5\sqrt{2363}\,\frac{\frac{1}{12}(12)(18.5)^3}{9.25(12000)} = 20.8 \text{ ft}\cdot\text{kip}\ (28.2 \text{ kN}\cdot\text{m}) \tag{39}$$

$$20.8 \text{ ft}\cdot\text{kip}\ (28.2 \text{ kN}\cdot\text{m}) < 22.6 \text{ ft}\cdot\text{kip}\ (30.6 \text{ kN}\cdot\text{m}) \quad \text{O.K.} \tag{40}$$

$$e_{bi} = \frac{M_{ip}(h - kd)}{I_{cr}E_c} \tag{41}$$

The multiplier on the beam depth, d, to find the cracked neutral axis position is k = 0.321. This produces a cracked moment of inertia I_{cr} = 2600 in^4 (108,220.17 cm^4). The strain level on the bottom of the slab at the time of FRP installation, thus becomes,

$$e_{bi} = \frac{(22.6 \text{ ft} \cdot \text{kip} \times 12 \text{in/ft})(18.5 - 0.321(16.75))}{(2600)(2771)} = 494\,me \qquad (42)$$

4.2. PRELIMINARY DESIGN

4.2.1. Ultimate Strength Analysis. The ultimate limit state analysis calculates the capacity of the section by combining force equilibrium, strain compatibility, and the constitutive laws of the materials at failure. The stress and strain distributions at ultimate are shown in Figure 4.2. The non-linear stress strain behavior of concrete may be replaced for computational ease by a rectangular stress block with dimensions $\gamma f'_c$ x $\beta_1 c$.

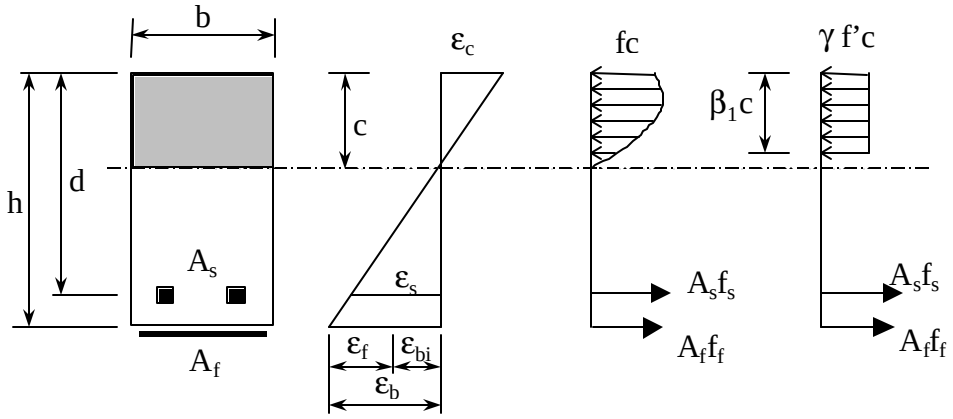

Figure 4.2. Strain and Stress Distribution in a RC Section at Ultimate

It should be noted that the Whitney stress block employed by ACI 318 is not valid when the concrete strain falls below 0.003 in/in (mm/mm). In this instance, the two most common representations of the stress-strain curve of concrete are the Modified Hognestad and Todeschini approximations. The Todeschini approximation (Todeschini et al. 1964) is the easiest to use and is readily adaptable to computer applications (MacGregor 1997).

The general equation for the nominal moment capacity of a RC section strengthened with FRP flexural reinforcement is given in Equation (43).

$$M_n = A_s f_s \left(d - \frac{ß_1 c}{2} \right) + 0.85 A_f f_f \left(h - \frac{ß_1 c}{2} \right) \qquad (43)$$

The term ƒs indicates the reinforcing steel is not necessarily at its yield stress. Addition of FRP to the beam may result in over-reinforcement for moment capacity thus the concrete may crush before the steel yields. The 0.85 factor applied to the moment contribution of the FRP reinforcement is additional to the three standard deviation reduction of the strength of the FRP. The additional 0.85-reduction term accounts for the novelty of the strengthening system and

performance under long-term conditions. There is discussion within the technical community and in particular within Committee 440 of the American Concrete Institute to arrive to a scientifically based expression of the reduction factor. The current thinking is that the material properties reported by manufacturers should be considered as initial properties that do not consider long-term exposure to environmental conditions. Because long-term exposure to various types of environments can reduce the tensile properties and creep rupture and fatigue endurance of FRP bars, the material properties used in design equations should be reduced based on the environmental exposure condition. The modulus of elasticity is unaffected by environmental conditions.

The stresses in each of the materials will depend on the strain distribution and the governing failure mode. Because of the number of variables involved, there is no direct procedure for determining the strain distribution and failure mode. Instead, a trial and error procedure is necessary. This procedure involves first estimating the depth to the neutral axis, c, and determining the failure mode based on this estimate. The estimated depth to the neutral axis may be confirmed or modified based on strain compatibility, the constitutive laws of the materials, and internal force equilibrium. In most situations, a first estimate of c = 0.15d is reasonable.

4.3. CFRP SELECTION

The "as built" moment capacity is 9% below the required moment capacity. Compensating for section losses, referenced in 4.1, an additional 10% will be added to the required moment capacity. It is reasonable to assume that externally bonded FRP sheets will be capable of correcting this deficiency. A commercially available FRP strengthening system (Mbrace™ Design Guide, 1998) was selected for its high strength and excellent performance under sustained and cyclic loading.

4.3.1. Estimate Amount of FRP Sheets Required. The first step was to estimate the area of FRP based on the additional tensile force, T, required to equilibrate the moment deficiency.

$$T = \frac{M_u - f\ M_n}{0.90 \cdot d} = \frac{((66 - 54.4) \times 12)}{0.90(16.75)} = 9.23 \text{ kips } (41.07 \text{ kN}) \quad (44)$$

$$A_{f,est} = \frac{T}{\phi \cdot 0.85 \cdot f_{fu}} = \frac{9.23}{0.90(0.85)(550)} = 0.0219 \text{ in}^2 \ (0.14 \text{ cm}^2) \quad (45)$$

Based on this area, the trial width of FRP becomes,

$$w_f = \frac{A_f}{n_p \cdot t_f} = \frac{0.0219}{1(0.0065)} = 3.37 \text{ in } \therefore \text{Try 1 ply, 4 in. wide; } A_f = 0.026 \text{in}^2 \quad (46)$$

Note: 1 in = 25.4 mm

The actual flexural capacity must now be computed.

4.3.2. Trial and Error Estimation. The first estimation of c = 0.15d which equates to c = 0.15(16.75) = 2.5125 inches (6.38 cm).

With the estimate of c, the failure mode may be checked by the following criterion:

- if $e_{fu} + e_{bi} > e_{cu}\left(\frac{h-c}{c}\right)$, failure is controlled by concrete crushing;
- if $e_{fu} + e_{bi} < e_{cu}\left(\frac{h-c}{c}\right)$, failure is controlled by FRP rupture.

For the estimated value of c,

$$e_{cu}\left(\frac{h-c}{c}\right) = 0.0191 \text{ in./in.} \tag{47}$$

$$e_{fu} + e_{bi} = 0.01549 \text{ in./in.} \tag{48}$$

therefore the failure mode is FRP rupture.

The strain level in the FRP, concrete and reinforcing steel is,

$$\varepsilon_f = \varepsilon_{fu} = 0.015 \tag{49}$$

$$e_c = \left(e_{fu} + e_{bi}\right)\left(\frac{c}{h-c}\right) = \left(0.015494\right)\left(\frac{2.5125}{18.5-2.5125}\right) = 0.00243 \text{ in./in} \tag{50}$$

$$e_s = \left(e_{fu} + e_{bi}\right)\left(\frac{d-c}{h-c}\right) = \left(0.015494\right)\left(\frac{16.75-2.5125}{18.5-2.5125}\right) = 0.01380 \text{ in./in} \tag{51}$$

which produces stress levels in the FRP and reinforcing steel,

$$f_f = f_{fu} = 550 \text{ ksi } (3{,}792.06 \text{ MPa}) \tag{52}$$

$$e_s \geq e_{sy} \therefore f_s = f_y = 30{,}000 \text{ psi } (206.84 \text{ MPa}) \tag{53}$$

The parameters that define the equivalent stress block are (Todeschini, 1964),

$$e_c' = \frac{1.71 \cdot f_c'}{E_c} = \frac{1.71(2363)}{57000\sqrt{2363}} = 0.001458 \text{ in./in} \tag{54}$$

$$\frac{e_c}{e_c'} = \frac{0.002435}{0.001458} = 1.67 \tag{55}$$

$$ß_1 = 2 - \frac{4\left[\left(e_c/e_c'\right) - \tan^{-1}\left(e_c/e_c'\right)\right]}{\left(e_c/e_c'\right)\ln\left(1 + e_c^2/e_c'^2\right)} = 2 - \frac{4\left[(1.67) - \tan^{-1}(1.67)\right]}{(1.67)\ln\left(1 + (1.67)^2\right)} = 0.851 \tag{56}$$

$$? = \frac{0.90\ln\left[1+\left(e_c^2/e_c'^2\right)\right]}{ß_1\left(e_c/e_c'\right)} = \frac{0.90\ln\left[1+(1.67)^2\right]}{(0.851)(1.67)} = 0.843 \quad (57)$$

Check the estimate on c,

$$c = \frac{A_s f_s + A_f f_f}{?f_c' ß_1 b} = \frac{1.53(30{,}000)+(0.026)(550)1000}{0.843(2363)0.851(12)} = 2.96\,\text{in.} \quad (58)$$

Note: 1 in. = 25.4 mm

2.96 in. ≠ 2.5125 in. ∴ A revision is required by iterating values of (c). Results are tabulated in Table 4.1.

Table 4.1. Summary of Trial and Error Calculations to Obtain c

c estimated (in)	Failure Mode	ε_{fu} (in/in)	f_f (ksi)	ε_s (in/in)	f_s (ksi)	ε_c (in/in)	β_1	γ	c calculated (in)
2.5125	FRP	0.015	550	0.01380	30	0.00244	0.851	0.843	2.957
2.8000	FRP	0.015	550	0.01377	30	0.00276	0.878	0.824	2.932
2.9300	FRP	0.015	550	0.01375	30	0.00292	0.890	0.813	2.931
2.9310	FRP	0.015	550	0.01375	30	0.00292	0.850*	0.813	2.931

* Limit to 0.85 as per ACI (Note: 1 ksi = 6.89 MPa; 1 in = 25.4 mm)

With the value of c as 2.93 inches (7.44 cm), compute the nominal moment capacity,

$$M_n = A_s f_s\left(d - \frac{\beta_1 c}{2}\right) + 0.85A_f f_f\left(h - \frac{\beta_1 c}{2}\right) \quad (59)$$

$$M_n = 1.53\frac{30000}{1000}\left(16.75 - \frac{0.85(2.931)}{2}\right) + 0.85(0.026)(550)\left(18.5 - \frac{0.85(2.931)}{2}\right) \quad (60)$$

$$M_n = 921\,\text{in}\cdot\text{kip} = 76.75\,\text{ft}\cdot\text{kip}\ (104.1\,\text{kN}\cdot\text{m}) \quad (61)$$

Because the strain in the steel at ultimate is much greater than twice its yield strain, the section retains sufficient ductility. The ϕ factor is therefore taken as 0.90.

$$\phi M_n = 0.90(76.75) = 69.1\,\text{ft}\cdot\text{kip} > M_u = 66\ \text{ft}\cdot\text{kip}\ \ (89.5\text{kN-m})\ \text{O.K.} \tag{62}$$

4.3.3. Check Shear Capacity. The shear capacity has been checked to ensure that it is greater than the factored ultimate shear force caused by an HS20. This requirement is defined by Equation (63):

$$\phi V_{n,existing} \geq V_u \tag{63}$$

4.3.4. Check Serviceability. Serviceability criteria include stress values, deflection and fatigue. This section only addresses the computation of stress in concrete, steel and FRP under service conditions. With respect to deflection, the use of FRP in this project was to correct a moment deficiency. Given the geometry of the deck, a serviceability limitation on deflections was not an issue. This is demonstrated by the extensive deflection measurements as reported in Chapter 6 of this report. Fatigue is not considered to be an issue based on the findings reported in Section 5.2 of this report.

By taking the first moments of the areas of concrete, steel (transformed to concrete), and FRP (transformed to concrete), the following expression is obtained:

$$\frac{(kd)^2 b}{2} - n_s A_s (d - kd) - n_f A_f (h - kd) = 0 \tag{64}$$

$$\frac{(kd)^2 12}{2} - \left(\frac{29000}{2771}\right)(1.53)(16.75 - kd) - \left(\frac{33000}{2771}\right)(0.026)(18.5 - kd) = 0 \tag{65}$$

Solving this quadratic, the depth to the neutral axis is kd = 5.53 inches (14.1cm) (k = 0.330). Compute the stress in the steel at a service moment of M_{serv} = 42 ft-kip (56.9 kN-m),

$$f_s = \frac{\left[M_{serv} + e_{bi} A_f E_f \left(h - kd/3\right)\right](d - kd) E_s}{A_s E_s \left(d - kd/3\right)(d - kd) + A_f E_f \left(h - kd/3\right)(h - kd)} \tag{66}$$

$$f_s = \frac{\left[42(12) + 0.000494(0.026)(33000)\left(18.5 - \frac{5.53}{3}\right)\right](16.75 - 5.53)(29000)(1000)}{1.53(29000)\left(16.75 - \frac{5.53}{3}\right)(16.75 - 5.53) + (0.026)(33000)\left(18.5 - \frac{5.53}{3}\right)(18.5 - 5.53)} \tag{67}$$

$$f_s = 21{,}862\ \text{psi} < 0.80 f_y = 24{,}000\ \text{psi}\ \ (165.47\ \text{MPa})\ \ \text{O.K.} \tag{68}$$

The current philosophy at UMR is to increase the allowable service load stress in the tensile reinforcement to 80 percent of yield as shown in Equation (68). This only applies when the flexural member is designed with conventional steel reinforcement and FRP is used to increase the flexural capacity.

Compute the maximum compressive stress in the concrete at service,

$$f_c = f_s\left(\frac{E_c}{E_s}\right)\frac{kd}{d-kd} = 21{,}862\left(\frac{2771}{29000}\right)\frac{5.53}{16.75-5.53} = 1030\text{ psi}\ \ (7.1\text{ MPa}) \tag{69}$$

$$f_c = 1030\text{ psi}\ (7.1\text{ MPa}) < 0.45f'_c = 1063\text{ psi}\ (7.3\text{ MPa}) \quad \text{O.K.} \tag{70}$$

Compute the stress in the FRP at service,

$$f_f = f_s\left(\frac{E_f}{E_s}\right)\frac{h-kd}{d-kd} - \varepsilon_{bi}E_f \tag{71}$$

$$f_f = \frac{21{,}862}{1000}\left(\frac{33{,}000}{29{,}000}\right)\frac{18.5-5.53}{16.75-5.53} - 0.000494(33000) = 12.46\text{ ksi}\ \ (85.8\text{ MPa}) \tag{72}$$

$$f_f = 12.46\text{ ksi} < 0.33C_DC_Ef_{fu} = 0.33(0.95)(0.65)550\text{ksi} = 112\text{ksi}\ \ (772.2\text{MPa})$$
$$\text{O.K. (Based on Mbrace}^{TM}\text{ guidelines)} \tag{73}$$

4.3.5. Automated Calculations. A computer program for the design of the CFRP strengthening with the Ultimate Strength Method with Service Load checking for serviceability was developed at the University of Missouri – Rolla. The program is reported in Appendix E. The program implementing the Ultimate Strength Method confirms the hand calculations previously reported. The minor differences are due to the method used to determine the concrete stress. The computer program uses the more exact method of integration to calculate the concrete stress. The hand calculations uses an approximate method whereby the area under the stress-strain curve is determined using the factors γ & β_1.

4.3.6. Conclusions. Based on the analysis, a single ply of FRP with a width of 4" per 12" (10.16 cm per 30.48 cm) width of slab would be sufficient to strengthen the bridge. This would correspond to a 10" (25.4 cm) wide single ply strip spaced at 30" (76.2 cm) on center for constructability and material economy. Because the FRP sheets to be used come in 20" (50.8 cm) wide rolls, these strips are easily field cut into halves without loss of material.

It is recommended that the distance between two adjacent strips (i.e., unreinforced area) be not larger than three times the depth of the concrete slab. This recommendation is consistent with conventional reinforced concrete practice.

After inspection of the bridge deck, it was noted that spalling of concrete due to steel reinforcement corrosion was visible at one edge of the slab. In order to apply CFRP on sound concrete without additional preparation work, it was decided to cluster the strips in the central portion of the deck, leaving a gap of 32.5 inch (82.5 cm) from each edge of the deck. Also it was decided to double the amount of FRP required by providing a total of eight 20 inch (50.8 cm) strips with a 3 inch (7.62 cm) gap between the strips, rather than using 10 inch (25.4 cm) strips. The final strengthening pattern is reported in Figure 4.3.

The excess FRP reinforcement was added for these reasons:

- Destructive pull-off testing was planned without compromising the integrity of the design.
- The fatigue testing had not been completed at the time of installation. It was elected to install additional FRP in the event that subsequent testing modified the original design. Once testing was completed and computations verified any excess FRP could be deactivated with transverse cuts in the fabric.

Even though at the end of the bond testing only the required FRP reinforcement will remain effective, doubling the amount of FRP does not change the failure mode due to FRP rupture. This is based upon the results from computations similar to those given in Appendix E (using a concrete strength of 2,750 psi = 18.9 MPa or higher), and laboratory verification on a test specimen equal to that described in Section 5.1 using twice the amount of FRP reinforcement. Also, at service load conditions, the change in stresses is minimal as indicated in below.

	Stress in psi		
	When FRP Required	When FRP Provided	Change (%)
Steel	21,851	21,636	-1.0
Concrete	1,030	1,033	0.3
FRP	13,091	12,825	-2.0

Note: 1,000 psi = 6.89 MPa

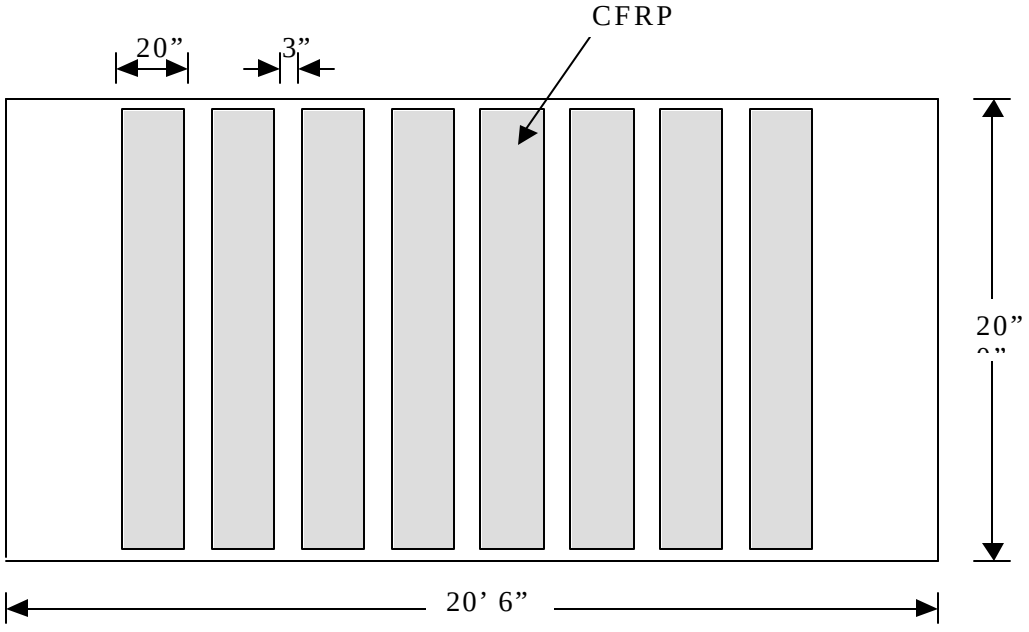

Note: 12 in = 1 ft = 304.8 mm

Figure 4.3. CFRP Strengthening Pattern

5. LABORATORY TESTING

5.1. FLEXURAL TESTING

5.1.1. Introduction. In order to verify the effectiveness of the strengthening system, it was decided to construct two full-scale RC beams that could be tested in the laboratory to failure. One was a control beam, the other one had to be strengthened with CFRP to achieve a 20% increase in flexural capacity. This would be the equivalent increase in strength needed in the existing structure, using MoDOT's rating criteria, to remove the load posting.

The dimensions of the test beams were chosen to mimic the existing bridge length of 20 feet (6.10 m) and the slab depth of 18.5 inches (0.47 m). A width of 15 inches (0.38 m) was chosen to provide an adequate surface area for the application of CFRP (Figure 5.1).

Copies of the original bridge plans were reviewed to determine the geometry, reinforcement layout and material properties of the bridge.

The bridge plans indicated that a 1:2:4 concrete mixture was used in the slab. The strength of a 1:2:4 concrete mixture depends on the material characteristics used, which were unknown. Coring the existing bridge deck was not feasible due to twelve inches of wearing surface. Next, an attempt was made to determine the concrete strength using a Schmidt hammer. Thirty tests were performed on the existing bridge slab and the results indicated the concrete had a compressive strength of 9,000 psi (62 MPa). This appeared excessive for concrete poured in 1922 even if one allows for some increase in strength due to aging. Finally, it was decided to use commercially available MoDOT standard Class B concrete. The estimated concrete strength of the two beams determined by standard cylinder breaks was 5,770 psi (39.8 MPa).

The reinforcement yield strength specified in the bridge plans was 30,000 psi (206.84 MPa). This presented a problem since reinforcing steel with yield strength of 30,000 psi (206.84 MPa) is no longer produced. Therefore, it was decided to use an area of steel such that the tensile capacity of the steel reinforcement in the beams was equal to that of the steel reinforcement in the bridge deck. As a result, it was decided to reinforce the two beams with two #5 rebars and two #6 rebars (total area of steel equal to 1.5 in^2 or 9.68 cm^2) of Grade 40 Steel. However, the rebars provided by the manufacturer were Grade 50 (#5) and Grade 80 (#6).

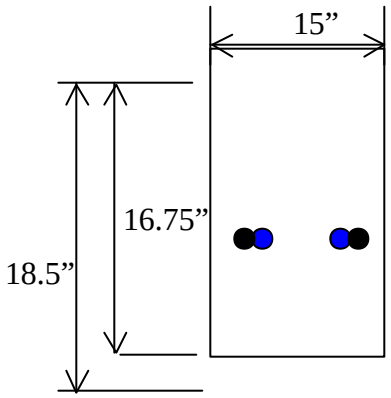

Note: 1in. = 25.4 mm

Figure 5.1. Cross-section of the Tested Beams

The amount of CFRP sheet to be used to strengthen one of the two beams was chosen in order to gain an increase in flexural capacity of about 20% with respect to the control beam. A 12 in. (0.305 m) wide strip of CFRP sheet was used. The material used was the same to be used in the strengthening of the bridge. According to the manufacturer, this CFRP sheet has a tensile strength of 550 ksi (3.79 Gpa) and an elastic modulus of 33000 ksi (227.5 Gpa) (MBrace ™ Design Guide, 1998).

5.1.2. Instrumentation. The beams were instrumented with strain gages attached to the internal reinforcing steel at mid-span and on the top compression face of the beam. Deflection measurements were recorded with LVDT gages placed at the supports, quarter points and at mid-span (Figure 5.2). The predicted maximum deflection was beyond the range of the LVDTs at mid-span. Additional deflection measurements were recorded manually using an Topcon™ automatic level. A load cell was placed on top of the hydraulic jack to measure the vertical force applied.

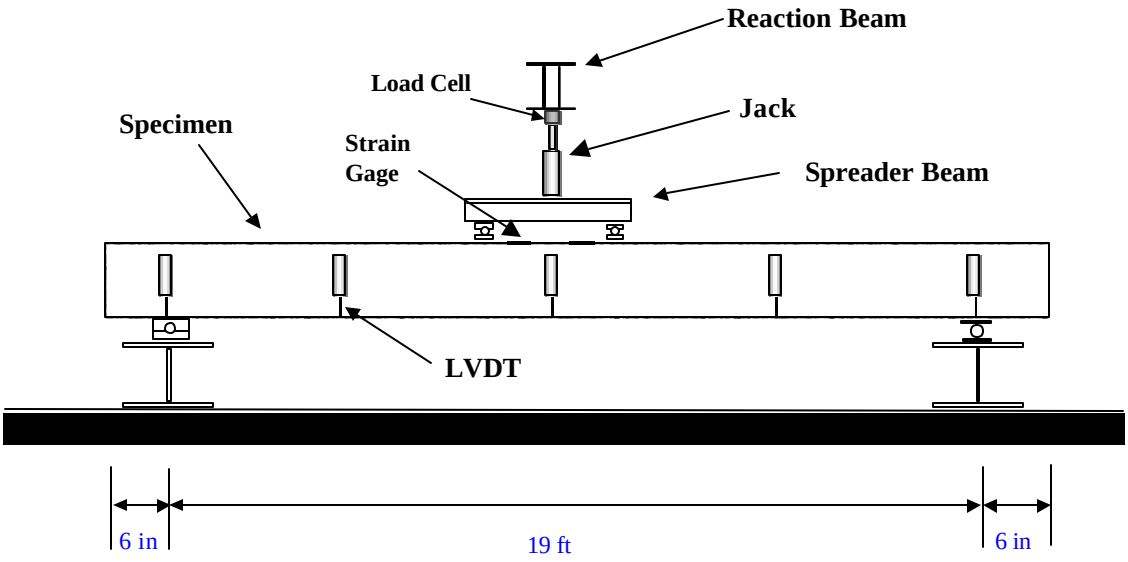

Note: 1 ft = 0.305 m

Figure 5.2. Test Setup

5.1.3. Loading Configuration. Loading of the beam was accomplished by the use of a 60 kip (267,000 N) hydraulic jack attached to an electric pump. The load cell on top of the jack, all LVDTs and strain gauges were attached to a data acquisition unit. The data acquisition unit continuously recorded all data while an increasing load pattern was used to load the beam. The load was increased in 5 kip (22,250 N) cycles until failure occurred.

5.1.4. CFRP Application Procedures. The bottom surface of the test beams was water blasted to remove laitance and surface contaminants then allowed to dry. A two-part epoxy primer was applied to the concrete surface where the FRP was to be applied and allowed to cure.

The next step was to apply epoxy putty that served to smooth out any remaining imperfections.

After the putty was applied and cured, the first coat of saturant was applied over the entire area that was to receive the FRP. Next the FRP sheet was measured, cut and applied. The FRP sheet was placed in contact with the concrete and pressed into the saturant in one continuous movement. To ensure proper embedment into the saturant and to remove any entrapped air, the entire surface of the FRP was pressed into the saturant with a small hand roller. The last step was to apply the final coat of saturant over the FRP. Primer, putty, saturant and CFRP sheet were the same materials used in the strengthening of Bridge G-270.

5.1.5. Test Results. A 27% increase in flexural capacity was achieved in the strengthened beam with respect to the control beam. The failure modes were crushing of the concrete and rupture of the FRP sheet for the unstrengthened and strengthened beam, respectively.

A theoretical analysis of the behavior of the two beams was carried out. The classical approach for RC sections was used, based on the assumption that plane cross-sections remain plane and on the principles of compatibility of strains and equilibrium of forces. In Figure 5.3 both the experimental and theoretical load-deflection curves are presented. The theoretical analysis allowed to predict accurately the load-deflection behavior, the ultimate load and the failure modes of the two beams.

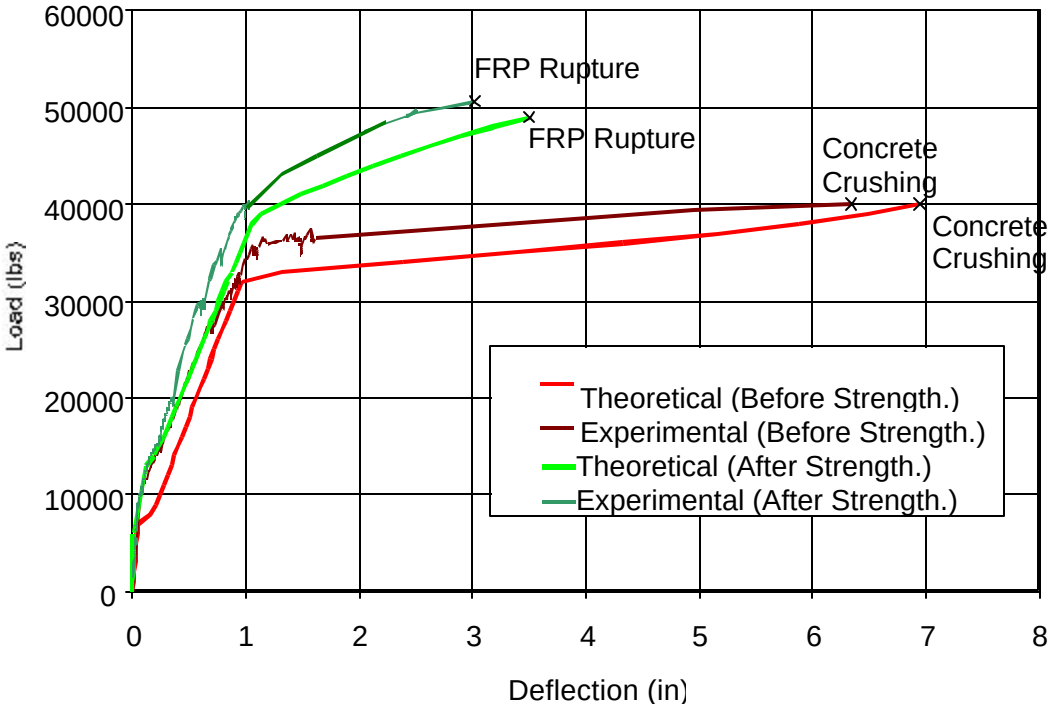

Note: 1 in. = 25.4 mm; 1 lb = 4.45 N

Figure 5.3. Load-Deflection Curves

The strengthened beam had a tighter cracking pattern and the FRP prevented the cracks from widening by preserving the aggregate interlock (Figure 5.4).

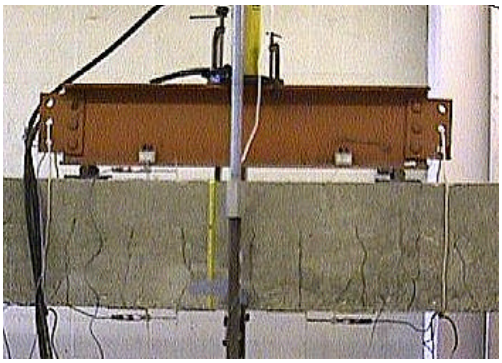

Control Beam

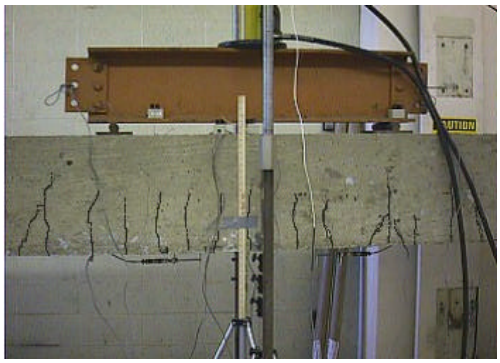

Strengthened Beam

Figure 5.4. Crack Pattern

5.1.6. Conclusions. The laboratory test of two full-scale beams, one unstrengthened and one strengthened with CFRP sheets, was conducted to verify the effectiveness of the strengthening technique. The dimensions of the cross-section, the concrete strength and the internal steel reinforcement were chosen to mimic the existing structure. Results showed that the expected increase in flexural capacity was achieved. The strengthened beam had a tighter cracking pattern and the FRP prevented the cracks from widening by preserving the aggregate interlock. The load-deflection behavior of the strengthened beam could be analytically predicted with good accuracy using the classic approach for RC sections.

5.2. FATIGUE TESTING

5.2.1. Introduction. The behavior of bond between FRP sheets and concrete is an issue in need of particular attention, since the bond is the means for the transfer of stresses from the concrete to the FRP reinforcement. The performance of bond under fatigue loading needs to be evaluated in order to achieve a safe design of the strengthening system. Therefore, experimental tests were performed to evaluate the behavior of bond of FRP sheets to concrete under fatigue loading. Details of the program and test results are presented in the following section.

5.2.2. Description of Specimen. Coupon-type specimens were used for this investigation. The specimen is a plain concrete beam with an inverted T-shape (Figure 5.5). The purpose of the T-shape is to provide a larger tension area for concrete while maintaining a manageable specimen size. A large tension area for concrete was required in order to avoid the occurrence of flexural cracking before failure of the bond. The beam is simply supported and has a span of 42 in. (1.07 m) and a total length of 48 in. (1.22 m). A notch was placed at the center of the beam in order to force the beam to develop only one crack at midspan. Also, a hinge was placed at the center of the beam. The purpose of the hinge was to cause the distance between the internal compression and tension forces to remain constant for any given load level. This allowed to compute accurately the tensile stress in the CFRP sheet at any load level.

One ply of CFRP strip was bonded to the tension face of the beam. Primer, putty, saturant and CFRP sheet were the same materials used in the strengthening of Bridge G-270. The sheet was 2 in. (5.08 cm) wide and had a fiber thickness of 0.0065 in. (0.165 mm). The modulus of elasticity of the fiber is 33,000 ksi (227.5 GPa). A transverse sheet was placed on one side to force failure to occur at the other end. Also, the sheet was left unbonded approximately 2 in. (5.08 cm) on

each side of midspan. The design choices were made to ensure that no flexural cracking would occur in the bonded area.

The above described specimen had been already used for a previous experimental program at the University of Missouri – Rolla (Miller, 1999). The topic of this program was the behavior of bond between CFRP sheets and concrete under static loading. The specimens were tested under four-point bending, with a shear span of 19 in. (48.26 cm). Among the specimens that had been tested, a series of specimens had one ply of CFRP sheet bonded to the bottom side and three different values of the sheet bonded length, namely, 4 in., 8 in. and 12 in. (10.16 cm, 20.32 cm and 30.48 cm , respectively). For the current program, a bonded length of 8 in. (20.32 cm) was adopted.

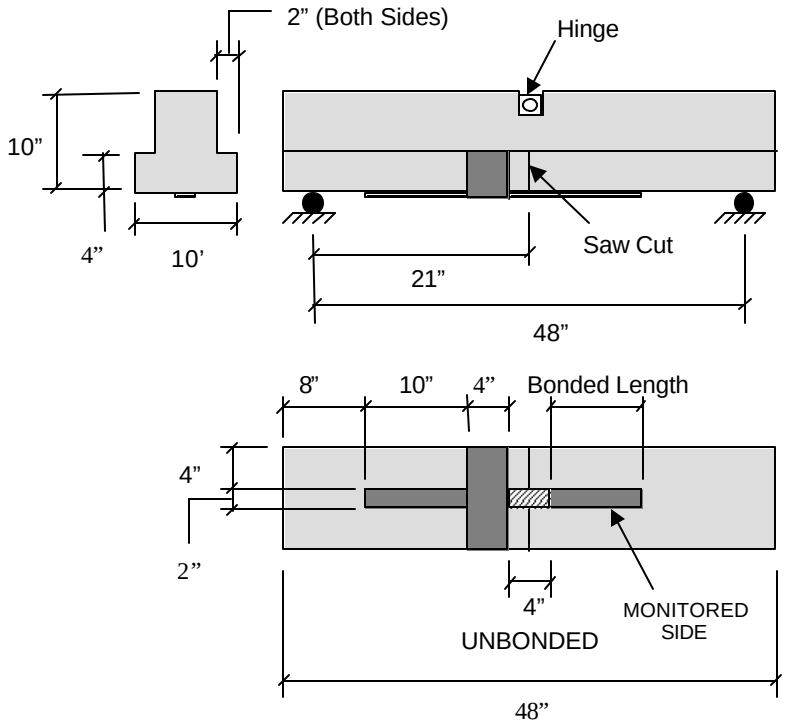

Note: 1 in. = 25.4 mm

Figure 5.5. Fatigue Test Specimen

In the tests performed by Miller (1999), the failure mode of the specimens was by peeling of the sheet. When comparing the results, it was found that the bonded length did not affect the bond strength. It was concluded that an effective length exists beyond which no stress is transferred until peeling occurs. The peeling mechanism was described as follows. The effective length of the CFRP sheet takes the entire load to a certain point at which localized peeling occurs causing the effective bond length to shift. This shifting of the effective bond length continues until the CFRP sheet has completely peeled from the concrete.

The value of load at which complete failure occurred was slightly higher than the load at which first peeling occurred. The latter load was evaluated from the strain vs. location diagrams as the load at which a linear shape of the strain distribution along the bonded length was observed. The

average values of first peeling load and ultimate load of all the specimens were 3,200 lbs (14,240 N) and 3,600 lbs (16,020 N), respectively. These two values of load correspond to a tensile stress in the FRP sheet of 267 ksi (1.84 GPa) and 301 ksi (2.08 GPa), i.e. to 49% and 55% of the tensile strength of the sheets as declared from the manufacturer (550 ksi or 3.79 GPa) (MBrace™ Design Guide, 1998).

5.2.3. Instrumentation and Test Procedure. When fatigue tests are performed, a remarkable number of parameters are involved and need to be appropriately chosen.

The most common approach to quantify fatigue behavior is the stress-life method. This method consists of load cycling the specimen at a constant amplitude stress range until failure or until a predetermined number of cycles is reached. The stress range is the range between a minimum stress, usually a small value, and a maximum stress. S_f is the ratio between the maximum stress applied during the fatigue loading and the ultimate stress under static loading. If each specimen is tested with a different value of the maximum stress, a stress-life diagram that plots S_f versus number of cycles to failure (N) results. Frequency of loading, stress ratio (minimum to maximum stress), and maximum stress are all parameters that may influence the fatigue life of the tested specimen.

In the present study, each specimen was subjected to cyclic loading under four point bending, with a shear span of 19 in. (0.48 m). It was decided that the maximum number of cycles to be applied be 2 million, assuming that no fatigue failure would occur afterwards. Although the service life of a bridge member exceeds 2 million cycles, this choice is believed to be reasonable to obtain reliable data while maintaining an acceptable duration of the laboratory tests.

The applied load was a sinusoidal function of time. The loading frequency was set at 5 Hz and the minimum stress was set equal to 5% of the failure stress under static loading. The tested specimens differed in the value of the maximum stress, which was equal to 60%, 75%, 80% and 90% of the first peeling stress under static loading. Table 5.1 summarizes the values of the testing parameters for the specimens. The test setup is shown in Figure 5.6.

Table 5.1. Parameters of Fatigue Testing

Specimen No.	Minimum Load (lbs)	Maximum Load (lbs)	Maximum Stress in the FRP Sheet (ksi)	Frequency (Hz)
1	175	1920	160	5
2	175	2400	200	5
3	175	2560	214	5
4	175	2880	241	5

Note: 1 lb = 4.45 N; 1 ksi = 6.89 MPa

Figure 5.6. Test Setup

A quasi-static test was performed on each of the specimens after different levels of fatigue conditioning, namely: 100,000, 200,000, 500,000 and 1 million cycles. The quasi-static loading was conducted up to the maximum load used in the cyclic conditioning. This allowed monitoring of bond behavior at different stages of conditioning and to have evidence of possible imminent peeling of the FRP sheets.

Strain gages were placed at different locations along the bonded and unbonded regions of the CFRP sheet, as shown in Figure 5.7. The purpose was to monitor the strain distribution along the bonded length of the sheet, from which the mechanics of the load transfer between the CFRP sheet and the concrete can be characterized. Data from the strain gages was recorded during each of the static tests, so that the strain distribution was monitored at different stages of fatigue conditioning.

For the specimens that survived 2 million cycles, static test to failure was conducted to determine the residual strength. Ultimate load and corresponding strain distribution were recorded.

5.2.4. Test Results. Three of the four specimens reached 2 million cycles without experiencing fatigue failure. Only the specimen conditioned at 90% of the first peeling stress failed after a fatigue conditioning of 120,000 cycles. The failure mode was peeling of the FRP sheet. These results are plotted in Figure 5.8. In the graph, S_f represents the ratio between the maximum stress applied during the fatigue conditioning and the peeling stress of the virgin specimen with no conditioning. N is the maximum number of cycles reached in the fatigue conditioning, in logarithmic scale. The arrows on the plotted points mean that no failure was experienced at that number of cycles.

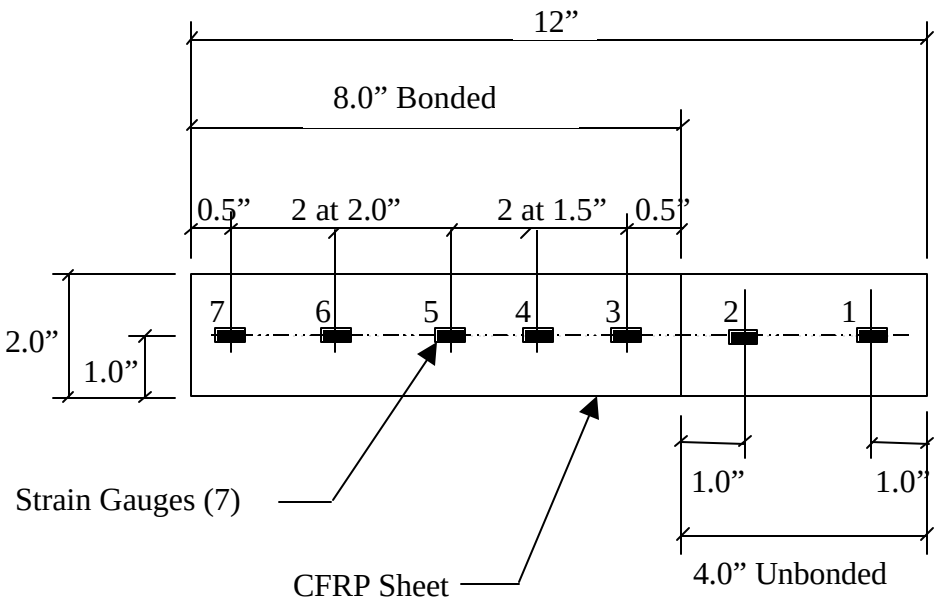

Note: 1 in. = 25.4 mm

Figure 5.7. Position of the Strain Gages

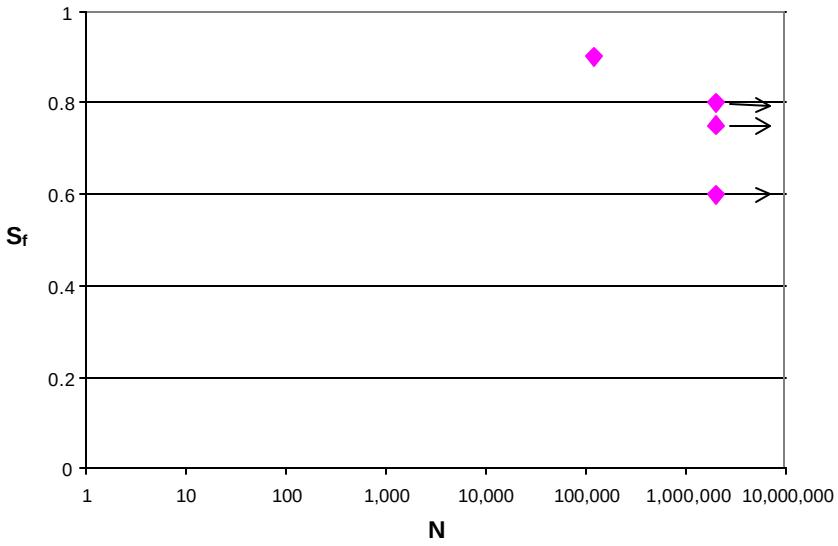

Figure 5.8. Stress – Life Diagram

The implication of these findings is that the endurance limit of externally bonded FRP, as far as bond failure is concerned, approaches the value of the static peeling strength. This statement is valid if the endurance limit is defined as the maximum stress applied in the cyclic loading corresponding to a fatigue life of 2 million cycles.

A quasi-static test up to the maximum load used in the cyclic conditioning was performed on each of the specimens after different levels of fatigue conditioning, namely, after 0, 100000, 200000, 500000 and 1 million cycles. Specimen No. 4 was statically tested after 0 and 100,000 cycles. For the specimens that survived 2 million cycles, a static test up to failure was performed after 2 million cycles were reached, to determine the residual strength.
Figure 5.9. shows the strain distribution in Specimen No. 3 at the maximum load used in the cyclic conditioning (80% of the static peeling load). The three curves refer to the specimen before any conditioning, after 1 million cycles and after 2 million cycles. No changes occurred in the strain distribution due to the fatigue conditioning.

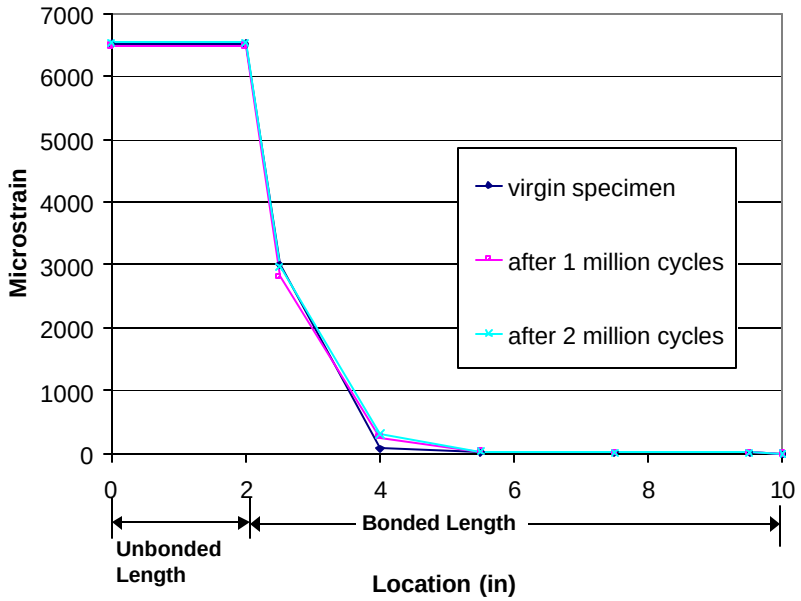

Note: 1 in. = 25.4 mm

Figure 5.9. Strain Distribution at Different Levels of Fatigue Conditioning (Specimen No. 3)

Figure 5.10 shows the strain distribution in Specimen No. 4 at the maximum load used in the cyclic conditioning (90% of the static peeling load). The two curves refer to the specimen before any conditioning and after 100,000 cycles. The notable change in the strain distribution gives evidence that damage of the bond is in progress.

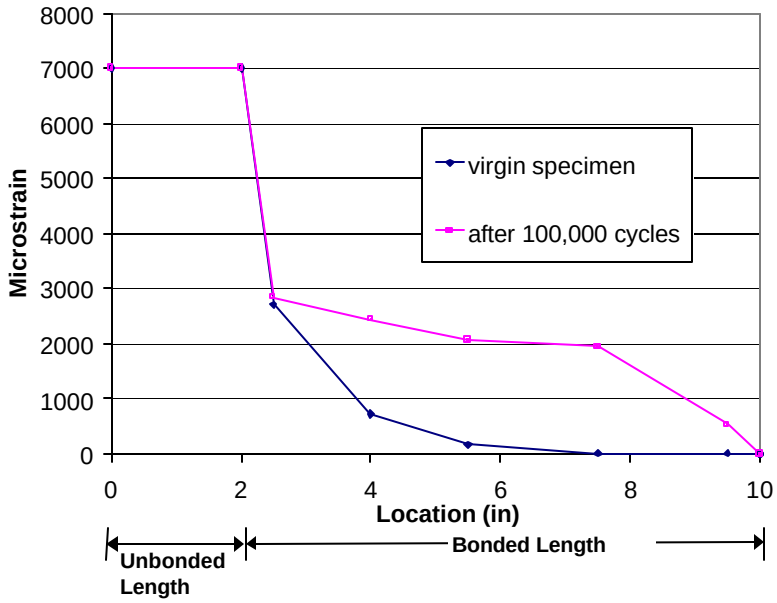

Note: 1 in. = 25.4 mm

Figure 5.10. Strain Distribution at Different Levels of Fatigue Conditioning (Specimen No. 4)

The specimens tested to failure after 2 million cycles failed by peeling of the FRP sheets, as did the virgin ones. The residual static strength of the specimens after 2 million cycles was higher than the strength of the virgin specimens. Furthermore, specimen No. 3 that had been load cycled up to the highest load showed the highest residual strength. The ultimate load of the specimens is reported in Table 5.2.

Table 5.2. Residual Strength of the Specimens After 2 Million Cycles

Specimen	Ultimate Load (lbs)	Stress in the FRP Sheet at Ultimate (ksi)	Ratio to the Nominal Tensile Strength (%)	Increase Over the Strength of the Virgin Specimens (%)
Virgin	3600	301	55	N/A
1	4050	338	61	12
2	3920	327	59	9
3	4430	370	67	23

Note: 1 lb. = 4.45 N; 1 ksi = 6.69 MPa

Figure 5.11 shows the strain distribution along the FRP sheet at ultimate. The two curves refer to the specimens tested under static loading and to specimen No. 3 of the ones tested after fatigue conditioning. Strain data regarding specimens No. 1 and 2 is not reported. The strain gages attached to the sheet in these specimens stopped working before the ultimate load was reached. The proper functioning of the strain gages was probably compromised by the fatigue loading.

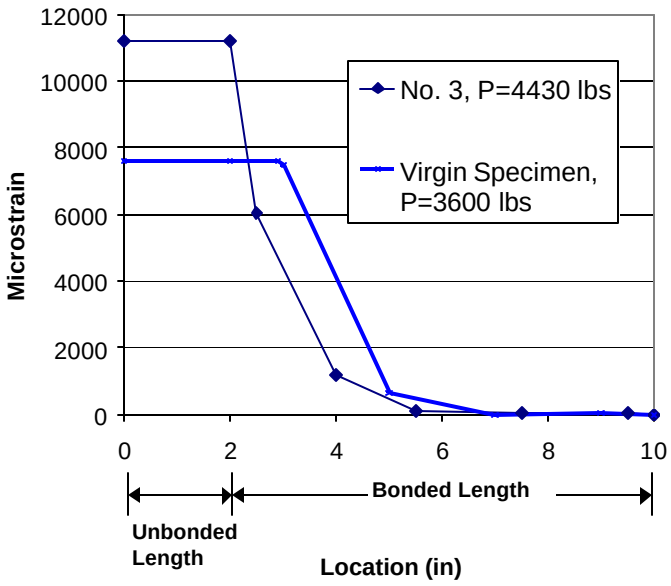

Note: 1 in. = 25.4 mm; 1 lb. = 4.45 N

Figure 5.11. Strain Distribution at Ultimate

The strain distribution in the virgin specimen clearly shows the occurrence of peeling, since strain is constant in the first region of the bonded length. This implies that detachment of the sheet from the concrete surface has started and will rapidly propagate along the entire bonded length. As far as specimen No. 3 is concerned, the strain distribution does not give evidence of peeling in progress. The peeling phenomenon was more sudden in the conditioned specimens than in the virgin ones, but the same sampling rate was used for data collection in both types of specimens. As a result, in the conditioned specimens the strain distribution during peeling was not captured.

From the strain distribution in specimen No. 3, it can clearly be seen that fatigue loading led to an improvement of the bond behavior with respect to the static specimens. Higher levels of load were reached before peeling of the FRP sheets started. Repeated loading led to modifications of the surface characteristics, which finally resulted in an enhancement of the bond behavior.

5.2.5. Conclusions. The behavior of bond between CFRP sheets and concrete under fatigue loading was investigated by testing coupon-type specimens. The cyclic conditioning was interrupted at 2 million cycles. Three of the four specimens did not fail under fatigue loading. The specimen load cycled at 90% of the load that produces bond failure under static loading failed after 100,000 cycles. A structural element in service under repeated loads is subjected to a load range which is very small compared to the load that would produce peeling of the FRP sheets. This value is typically less than 10% of the stress corresponding to peeling under static

loading. Therefore, results of the experimental tests seem to indicate that bond failure due to fatigue loading should not be an issue.

A static test up to failure was performed on the specimens that survived 2 million cycles. Results show that the residual static strength of the specimens after 2 million cycles is higher than the strength of the specimens subjected only to static loading. Furthermore, the specimen that had been load cycled up to the highest load showed the highest residual strength. Additional specimens could be tested to verify these results.

6. APPLICATION OF CFRP AND FIELD TESTING

In-situ load test was performed before and after the application of the FRP. The initial load test was performed on May 20, 1998. Immediately after the test was performed the contractor began applying the FRP. The University of Missouri-Rolla performed a second load test on August 19, 1999.

6.1. APPLICATION OF CFRP

The bottom surface of the bridge slab had form lines left from the original construction. These were ground smooth with hand grinders and the entire slab was lightly sand blasted to remove any loose material and laitance.

The next step was to mark the location where the FRP was to be applied. The centerline of the slab was identified and the locations of the FRP sheets were laid out. The layout pattern consisted of eight sheets of FRP, 20 in. (50.8 cm) wide, alternating with a 3-in. (7.62 cm) gap. Six sheets were used for strengthening, the two additional sheets of FRP were added for destructive test purposes. Bond tests are to be performed over the next few years on these two additional sheets.

A two-part epoxy primer was applied to the concrete surface to be covered with FRP and allowed to cure approximately twelve hours. The next step was to apply epoxy putty that served to smooth out any remaining imperfections. Immediately after the putty was applied, the first coat of saturant was applied over the entire area that was to receive the FRP (Figure 6.1). Next, a strip of FRP was measured, cut to length and applied in a fashion similar to wallpaper (Figure 6.2). One end of the FRP sheet was placed on the slab and pressed into the saturant. A second person applied the remainder of the sheet forcing it into the saturant in one continuous movement. To ensure proper embedment into the saturant and to remove any entrapped air, the entire surface of the FRP was pressed with a small hand roller. The last step was to apply the final coat of saturant over the sheet.

6.2. UMC INSTRUMENTATION

The load testing equipment used to determine the elastic deflection response was provided by the University of Missouri-Columbia. The equipment consisted of a self-supporting data acquisition vehicle with the capabilities of monitoring 100 channels of strain and 25 channels of deflection. The vehicle used to load the bridge consisted of a flatbed truck loaded with steel weights. The load test vehicle, totalling 21.14 tons (188,146 N), had known axle weights of 10,200 lbs. (45,390 N) front, 16,280 lbs. (72,446 N) and 15,800 lbs. (70,310 N) for the rear axles as shown in Figure 6.3. The data was collected with five LVDTs placed at quarter points both longitudinally and transversely. The locations of the LVDTs are shown in Figure 6.4.

Figure 6.1. Application of the Saturant

Figure 6.2. Installation of the CFRP Sheets

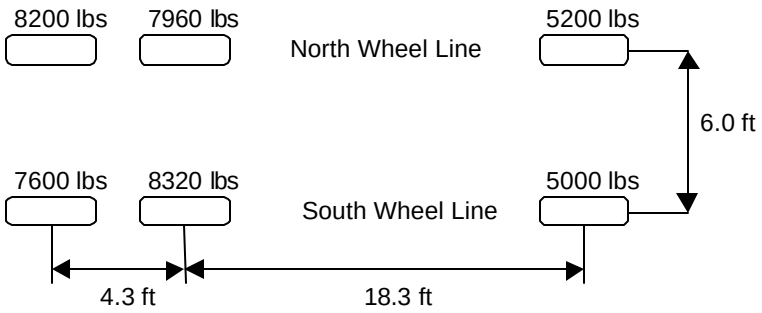

1 lb = 4.45 N; 1 ft. = 0.3048 m

Figure 6.3. UMC Test Truck Wheel Loads

6.3. UMC LOAD TESTING

A load test was performed on the bridge before and after the application of FRP. Deflection tests were performed by driving the loaded truck over the bridge. The test truck made six passes over the bridge. The truck drove forward and backward on the South side, North side and centerline of the bridge. Each time the truck passed over the bridge the deflection readings were measured and recorded. A typical load-deflection pattern is shown in Figure 6.5. The LVDT numbers correspond to those shown in Figure 6.4.

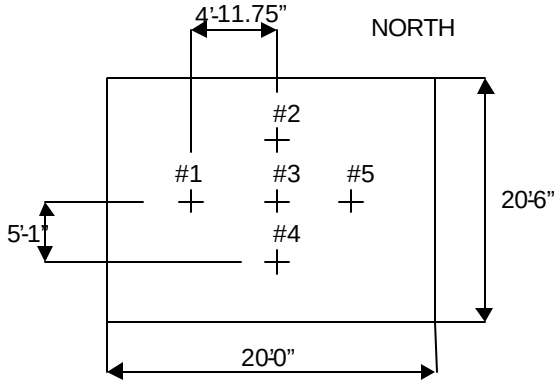

Note: 1 ft = 0.3048 m

Figure 6.4. LVDT Layout

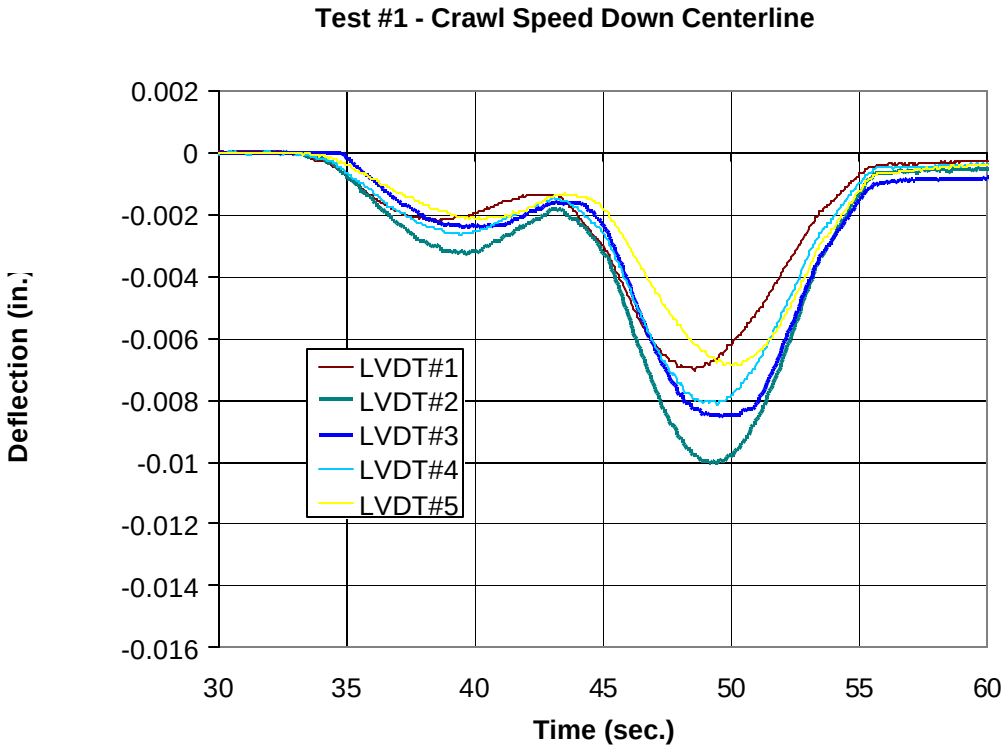

Note: 1 in = 25.4 mm

Figure 6.5. Deflections with Truck Driving Down Center of Bridge

6.4. LOAD DEFLECTION CHARACTERISTICS

Table 6.1 contains the tabulated results of the bridge deck deflections before and after strengthening. The average deflection measurements after strengthening were 94% of the original.

As seen from the data, deflections were not uniform. The North side of the bridge deck had some deterioration and spalling which produced the area of greatest deflections. This area, as a result of strengthening, showed the greatest reduction in the amount of live load deflection.

Table 6.1 Maximum Deflections Before and After Strengthening

Bridge Condition	Truck Path	LVDT Deflections (inches)				
		#1	#2	#3	#4	#5
Original (Before)	North	0.0068	0.0143	0.0087	0.0054	0.0067
	Middle	0.0070	0.0098	0.0091	0.0080	0.0069
	South	0.0059	0.0064	0.0074	0.0092	0.0058
Strengthened (After)	North	0.0063	0.0130	0.0086	0.0051	0.0063
	Middle	0.0067	0.0086	0.0090	0.0080	0.0066
	South	0.0054	0.0049	0.0073	0.0095	0.0054
After/Before Ratio (%)	North	93	91	99	94	94
	Middle	96	88	99	100	96
	South	92	77	99	103	93

Note: 1 in = 25.4 mm

6.5. UMR INSTRUMENTATION

The University of Missouri-Rolla provided the load testing equipment used on the second test to determine the elastic deflection response. The equipment consisted of a self-contained data acquisition unit with the capabilities of monitoring 5 channels of strain and 14 channels of deflection. The vehicle used to load the bridge consisted of a MoDOT dump truck loaded with gravel. The load test vehicle, totaling 23.02 tons (204,878 N), had known axle weights of 14,100 lbs. (62,745 N) front, 15,970 lbs. (71,067 N) for each of the rear axles as shown in Figure 6.6. The data was collected with five LVDTs placed at quarter points both longitudinally and transversely. The locations of the LVDTs are shown in Figure 6.7.

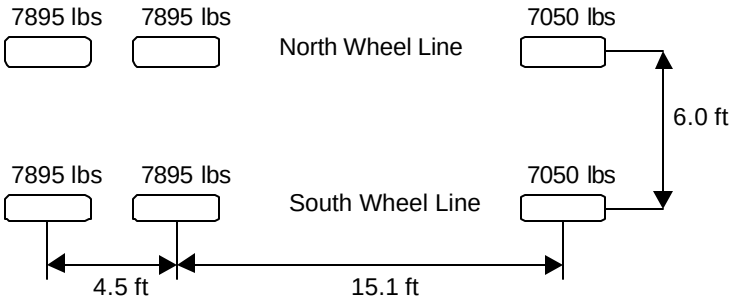

Note: 1 lb = 4.45 N, 1 ft = 0.3048 m

Figure 6.6. UMR Test Truck Wheel Loads

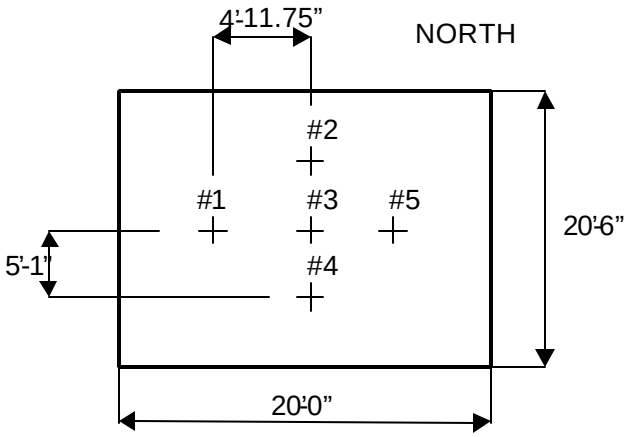

Note: 1 ft = 0.3048 m

Figure 6.7. LVDT Layout

6.6. UMR LOAD TESTING

A second load test was performed on August 19, 1999 after the application of FRP. This test was conducted to investigate the effects of time on the performance of the system. Deflection tests were performed by driving the loaded dump truck over the bridge. The test truck made three

passes over the bridge. The truck drove forward on the South side, centerline, and North side of the bridge. Each time the truck was positioned at the 1/4, 1/2, and 3/4 span points over the bridge. The truck was stopped for two minutes while the deflection readings were measured and recorded.

6.7. LOAD DEFLECTION CHARACTERISTICS

Table 6.2 contains the tabulated results of the deflection tests. As seen from the data, deflections were not uniform. The North side of the bridge deck had some deterioration and spalling and produced the area of greatest deflections.

Table 6.2 Maximum Deflections After Strengthening

Bridge Condition	Truck Path	LVDT Deflections (inches)				
		#1	#2	#3	#4	#5
Strengthened (After)	North	0.0063	0.0124	0.0080	0.0052	0.0062
	Middle	0.0068	0.0093	0.0090	0.0079	0.0067
	South	0.0052	0.0052	0.0074	0.0091	0.0052
$2^{nd}/1^{st}$ Test Ratio (%)	North	100	95	93	102	98
	Middle	101	108	100	99	102
	South	96	106	101	96	96

Note: 1 in = 25.4 mm

The results of the second load-deflection tests clearly show the FRP sheets continue to carry tensile stresses. The deflections are virtually the same as those taken by UMC on May 21, 1998 just after the FRP was applied. The average deflection measurements of the second test were 99.5% of the after strengthening tests performed by UMC. The results correlate well since the total weight of the test vehicles rear axles weighed within 500 lbs. (2.2 kN) of each other.

6.8 CONCLUSIONS

Installation of the CFRP sheets was simple and fast. Any construction worker can perform this type of work with proper training and supervision.

The performed load tests indicated a slight increase in stiffness of the structure as a result of the strengthening. The increase may appear insignificant, but this result clearly shows that the FRP sheets are carrying tensile stresses. The best indicator of the performance of the FRP reinforcement would be the measurement of the actual strain in the material under loading. Section 7.2 in this report addresses this issue.

7. LONG TERM MONITORING

7.1. MONITORING OF DURABILITY

7.1.1. Introduction. The objective of this investigation was to study the inadvertent electrochemical effects of CFRP materials on the degradation of reinforcing steel and vice-versa in a real service environment. The carbon material, very noble by nature, may pose a galvanic corrosion problem in the presence of a less noble material such as reinforcing steel, if there is a conductive environment. The effects of the CFRP composite material on steel are still not very clear and, so far, the system (CFRP repair material on RC) seems to work well due to the protective nature of the epoxy matrix material, which acts as a barrier. Until now, there has not been an opportunity for testing the whole system in a real-life application. From the corrosion study, it is expected to get some data that would be useful for recognizing the long-term effects of the CFRP materials on reinforcing steel, the environmental effects on CFRP materials, and the effect of system loading combined with environmental attack on CFRP.

As part of the strengthening efforts of Bridge G-270, in-situ corrosion measurements were planned. Since there is a possibility that the reinforcing steel may react with the carbon fibers, the interaction between these materials was monitored. The first approach included "corrosion potential measurements". Then, with use of a portable potentiostat, electrochemical impedance spectroscopy tests (EIS) were conducted. In this procedure, a small AC voltage is applied and impedance response is analyzed. With this technique, it is possible to monitor the electrochemical degradation occurring on the steel and on the CFRP. Finally, the polarization resistance method was also employed.

7.1.2. Measurements on Bridge G-270. The first set of data was collected on May 20-21, 1998. Corrosion potential measurements, polarization resistance and EIS measurements were conducted. In order to establish electrical connection between the reinforcing steel and potentiostat leads, four holes were drilled on various points under the bridge. Two holes were near the North edge of the slab and the others were in the middle of the slab. The North edge of the slab has spalling and some visible corrosion of the internal steel reinforcement (Figure 7.2), while the South edge had good surface integrity (Figure 7.1).

Four points were chosen at two-foot intervals along each reinforcing bar to collect the data. A letter A or B designates these points. Thus, a number, the number representing the reinforcing bar location where the working electrode was connected, and the letter representing the location where the reference electrode was coupled, will identify each measurement. The location of the exposed reinforcing bars and the data collection points are shown in Figure 7.3.

The collection of data had to be stopped during polarization resistance experiments and duplicate EIS due to flooding. The analysis of the results of this testing has produced a reasonable and reliable set of corrosion potential measurements. The polarization resistance and EIS measurements produced unintelligible results during this test for several reasons, including: the difficulty of holding the electrodes in position without disturbance during the testing, the premature ending of the testing program due to flooding at the bridge site, problems obtaining electrical contact with the electrodes, and the general difficulty of obtaining reliable measurements in the field.

Figure 7.1. Condition of South Side

Figure 7.2. Corrosion on North Side

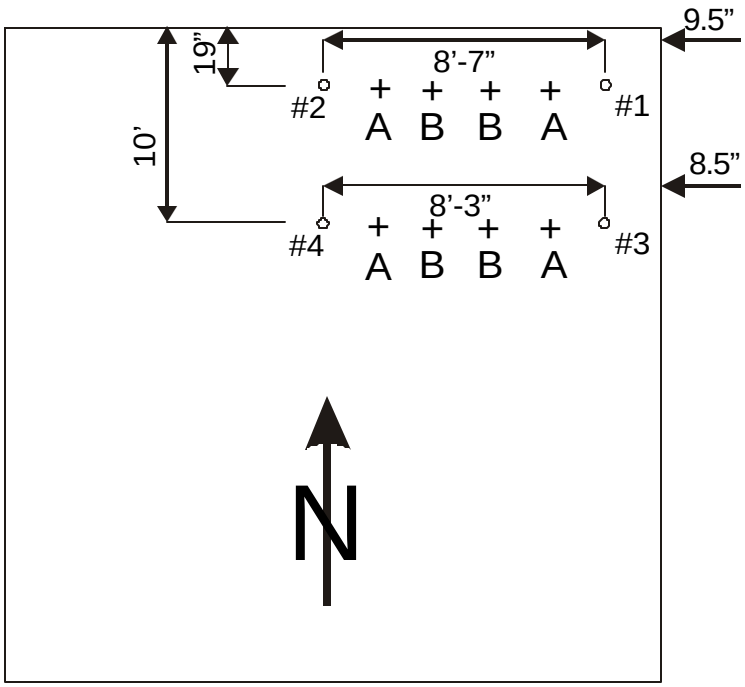

Note: 1 ft = 12 in = 304.8 mm

Figure 7.3. Location of Test Points on Underside of Bridge G-270

The bridge was re-visited on May 30, 1999. At this time only points 1 and 3 were accessible to testing due to stream flow. Reliable measurements of corrosion potential and of polarization resistance were obtained. The corrosion potential measurements are summarized in Table 7.1, and the polarization resistance measurements are summarized in Table 7.2.

Table 7.1. Corrosion Potential Measurements

Point	May 1998 E_{corr} (mV) (re $Cu/CuSO_4$)	May 1999 E_{corr} (mV) (re $Cu/CuSO_4$)
1A	-202	-560
1B	-215	-222
2A	-227	
2B	-260	
3A	-40	-9
3B	-80	-63
4A	-55	
4B	-60	

Table 7.2. Polarization Resistance Measurements

Point	May 1999 i_{corr} (amp/cm^2)	May 1999 R_p(Ωcm^2)
1A	5.8×10^{-7}	4.5×10^{4}
1B	2.0×10^{-7}	1.3×10^{5}
2A		
2B		
3A	1.0×10^{-6}	2.6×10^{4}
3B	2.1×10^{-6}	1.2×10^{4}
4A		
4B		

Note: 1 cm = 0.394 in

7.1.3. <u>Findings.</u> The duplication of the corrosion potential measurements provides a basis for initial evaluation of the long-term electrochemical effects on the bridge. Table 7.1 presents comparisons of the measurements from 1998 and 1999. The potential readings are similar, with a possible slight increase in the potential from 1998 to 1999. One exception is the readings at point 1A, where the potential dropped dramatically over the year between observations.

The 1999 polarization resistance measurements, presented in Table 7.2, provide an indication of the actual rate of corrosion, in addition to the potential for corrosion. The corrosion current i_{corr} and the polarization resistance R_p, given in the table for points 1A, 1B, 3A, and 3B, can be converted to a rate of corrosion, if the conductive area on the surface of the bar is known. Since the conductivity of the bar is established by wetting through the concrete, it is impossible to have a precise measurement of this area. For a 0.167 $in.^2$ (1 cm^2) area, the corrosion at point 1A represents a rate of 7µm per year, whereas for a 0.167 $in.^2$ (1 cm^2) area, the corrosion at point 3B is 21µm per year. A larger conductive area would reduce this result, and a smaller area would increase it.

The bar at the interior of the bridge, with points 3 and 4 was in a passive state in the 1998 testing, and remained so through the summer of 1999. The bar towards the edge of the bridge, with points numbered 1 and 2 has been corroding continually for the duration of the testing program. The corrosion potential of the bar has increased dramatically near point 1 during the yearlong duration of the testing program.

The polarization resistance results are very difficult to interpret as absolute results for two reasons. First, the wetted area of the bar surface is unknown, and second, it is not possible to separate the resistance of the medium (concrete) from the resistance at the surface of the bar. The results are generally indicative of moderate corrosion rates, with further damage expected within the next 10 to 20 years.

It will be possible in the future to compare future polarization resistance measurements with the current measurements. It will also be possible in the future to take electrochemical impedance spectroscopy measurements. These are capable of isolating the effect of concrete from the effect of the steel. Use of EIS will improve the data that can be obtained from field measurements, since once the ohmic resistance value of the concrete is known, it is possible to interpret the polarization resistance data and obtain realistic corrosion rate calculations.

7.2. MONITORING OF STRAIN

7.2.1. Smart Sensing Experimental Plan. A fiber-optic strain sensing capability was added to the FRP reinforcement of the bridge. The objectives of this work were to demonstrate the fiber optic sensor compatibility with FRP reinforcement of a concrete bridge, and to facilitate long-term monitoring of the integrity of the FRP reinforcement. The sensors were designed for static strain measurements and were extrinsic Fabry-Perot interferometric (EFPI) type devices manufactured by F&S, Inc. (model AFSS). These sensors provide a point measurement of strain with little perturbation to the host structure, resistance to corrosion and fatigue, and high sensitivity. They had a gauge length of 0.197 in. (5 mm), a resolution of about 5 microstrain, and a maximum strain of about 5000 microstrain.

Fiber optic strain sensors were installed in both the concrete soffit and the FRP plies at several locations. The purpose was to characterize the load-induced strain by comparing the readings in the concrete and the FRP at similar locations. Changes over time, if any, would non-destructively evaluate the aging of the FRP-concrete bond. It is envisioned that information will be collected from the sensors in the future years to obtain a long term monitoring of the structure.

7.2.2. 1998 Installation. Twelve fiber optic sensors were installed in the spring of 1998 during the FRP placement. Four pairs (one in the concrete soffit and one on the FRP) were placed in the mid-span of the bridge. Another pair was placed 14.96 in. (38 cm) from the abutment. Also, two sensors were placed in the South side of the deck at mid-span, one near the upper surface and one near the lower surface. All paired sensors in concrete were placed in a 0.118 in. (3 mm) deep groove to isolate the measurement from the FRP above. The fiber lines were bonded to the surface of the FRP or concrete. A junction box was attached to the abutment to provide access to the fiber lines. Figure 7.4 shows the attached box during the sensor installation. The loose lines were later bonded to the abutment.

The sensors were tested after installation and a baseline strain recorded. All sensors were functioning. Between the installation and the load first load test, vandals destroyed all of the fiber optic sensors. The fiber lines were pried away from the abutment and severed. None of the fiber lines had enough length to reattach a termination.

Figure 7.4. Junction Box of the Fiber Optic Sensors

7.2.3. 1999 Installation. Four replacement fiber optic sensors were installed during the summer of 1999. Two pairs (one in the concrete soffit and one on the FRP) were placed in the mid-span of the bridge (Figure 7.5). All paired sensors in concrete were placed between the FRP reinforcement strips. (The sensors could not be placed under the existing FRP.) Sensors were placed on the FRP surface 0.79 in. (2 cm) from the edge of the strip and 1.57 in. (4 cm) from the corresponding concrete sensor. All fiber lines were placed in 0.118 in. (3 mm) deep grooves. The grooves ran from the sensor head to the junction box. The FRP sensor lines were routed to the concrete groove within 1.97 in. (5 cm) of the sensor head. To discourage vandalism, the grooves were covered with a concrete patch material. Also, the fiber line entered the back of the junction box and the box was located on the abutment next to the creek channel. It is envisioned that periodic load tests will be conducted on the structure in the future. Information will be collected from the sensors at each load test to monitor strain changes in time. A potential duration of five years for the monitoring is envisioned.

7.3. DIRECT TENSION PULL-OFF TEST

7.3.1. Scope and Objective. This test method is based on ACI 503R-93 and ASTM D 4541. This is the "Standard Test Method for Pull-Off Strength of Coatings Using Portable Adhesion Tester". This test is supplemented with the requirement to use a portable adhesion tester with a 2 square inch (1290 mm^2) adhesion-loading fixture, Figure 7.6, with an adjustable and smooth force pull-off rate. This portable pull-off test is a means to uniformly prepare and test the tensile bond strength of an FRP laminate bonded to the surface of a concrete member and/or test the tensile strength of the substrate concrete.

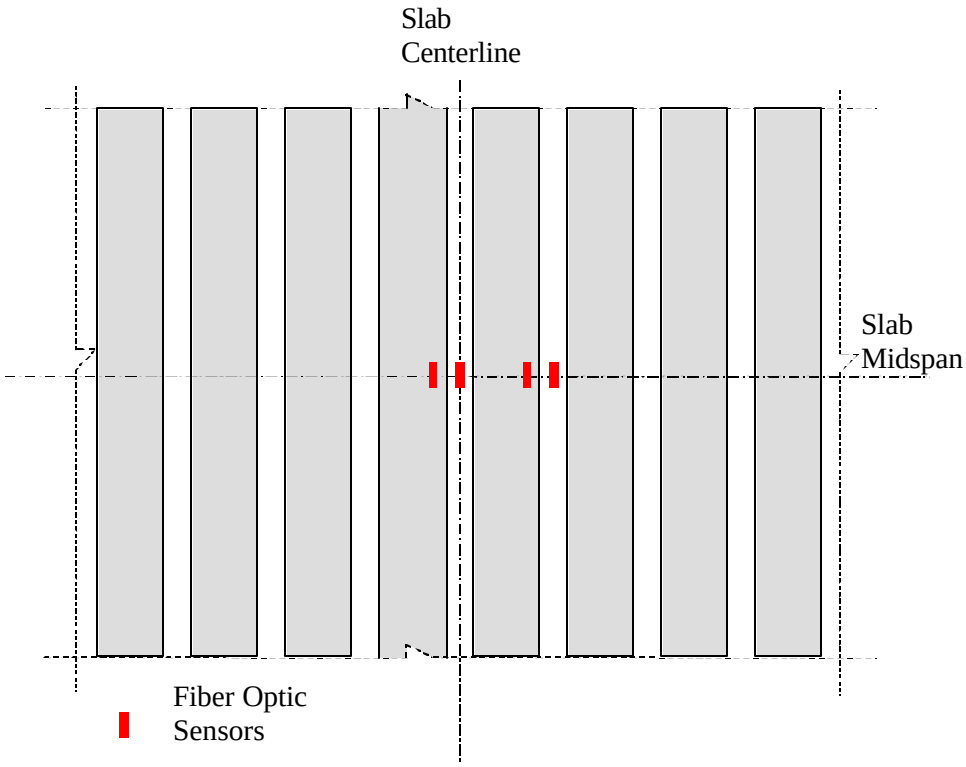

Figure 7.5. Location of Sensors on Underside of Bridge G-270

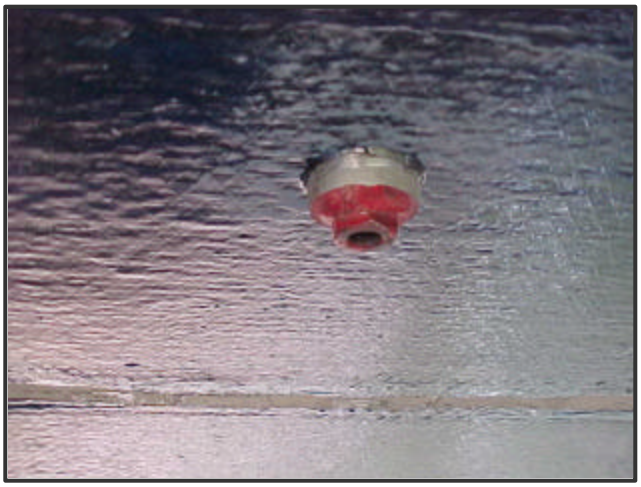

Note: 1 in^2 = 645.2 mm^2

Figure 7.6. Two Square Inch Adhesion Fixture

7.3.2. Field Test. Six pull-off tests were performed on October 15, 1998. The first six adhesion fixtures (Figure 7.6) were attached to the surface of the FRP with epoxy adhesive. The locations of the test are shown in Figure 7.7. After the epoxy adhesive cured a core drill (Figure 7.8) was used to isolate the adhesion fixture from the surrounding FRP. Next the test apparatus was attached to the adhesion fixture and aligned to apply tension perpendicular to the concrete (Figure 7.9).

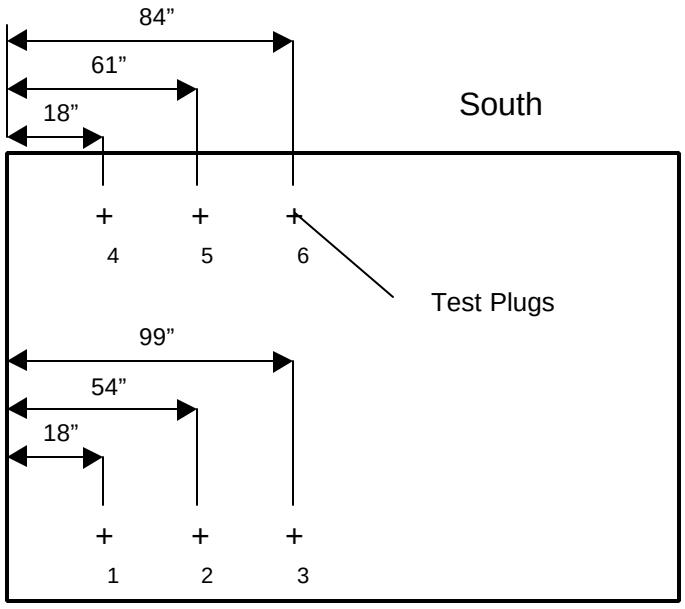

Note: 1 in = 25.4 mm

Figure 7.7 Pull-off Test Locations

Figure 7.8. Core Drill

Figure 7.9 Pull-off Test Apparatus

A constant force rate was applied to the adhesion fixture and recorded until the adhesion fixture detaches from the surface. There are three basic types of failure modes:

- Concrete - Concrete fails in tension
- Epoxy - Epoxy glue attaching the adhesion fixture to the FRP fails
- FRP - FRP delaminates from the concrete.

The pull-off strength shown in Table 7.3 was computed based on the maximum indicated load. The results show good adhesion between the FRP and the concrete substrate. In fact, the two failure mechanisms recorded (i.e., epoxy and concrete) indicated that the FRP concrete interface was stronger than either the concrete substrate itself or the glue used for the fixture. Figure 7.10 shows an adhesion fixture with concrete attached, i.e. concrete failure mode. Typically, externally bonded FRP should be attached to a concrete substrate that has a pull-off strength higher than 200 psi (1.38 MPa). These tests indicate that substrate and FRP bond to concrete are more than acceptable.

It is envisioned that periodic pull-off tests will be conducted on the FRP in the future. Information will be collected from each pull-off test to monitor any bond changes over time. A potential duration of five years for the monitoring is envisioned.

Table 7.3 Pull-Off Test

Location	**Pull-Off Strength** (psi)	**Failure Mode**
1	600	Epoxy
2	700	Epoxy
3	600	Epoxy
4	400	Concrete
5	300	Epoxy
6	900	Concrete

Note: 1000 psi = 6.89 MPa

Figure 7.10. Adhesion Fixture Showing Concrete Failure Mode.

8. CONCLUSIONS

The results of a pilot study to apply externally bonded CFRP sheets to strengthen a simple span reinforced concrete solid slab bridge were presented. The ultimate goal was to increase the load carrying capacity of the structure and to allow the removal of the restricted load posting. Verification on the effectiveness of the strengthening system was accomplished by laboratory testing of two full-scale beams and in-situ field tests of the actual bridge before and after strengthening. Information on the long-term behavior of the strengthened bridge was gained by laboratory fatigue testing of coupon-type specimens and by monitoring of durability and strain condition of the real structure. The following conclusions could be drawn:

- Externally bonded CFRP sheets are an effective technique to enhance the flexural capacity of RC beams. The laboratory test of two full-scale beams, one unstrengthened and one strengthened with CFRP sheets, showed that the expected increase in flexural capacity was achieved. The load-deflection behavior of the strengthened beam could be analytically predicted with good accuracy using the classic approach for RC sections as shown in Figure 5.3.
- The bond between CFRP sheets and concrete exhibits a very good behavior under fatigue loading. Results of laboratory tests conducted on coupon-type specimens showed that the endurance limit of externally bonded FRP (defined at 2 million cycles), as far as bond failure is concerned, approaches the value of the static peeling strength. The residual bond strength after 2 million cycles was higher than that of the virgin specimens.
- Externally bonded CFRP sheets can produce an increase in the stiffness of the structure. The average deflection measurements after strengthening were 94% of the original. The greatest reduction in the amount of live load deflection was obtained in the side of the bridge deck that had showed the greatest deflections before strengthening due to some deterioration and spalling.
- The results of the durability monitoring obtained so far are generally indicative of moderate corrosion rates. Further monitoring of durability and strains is envisioned for the future years.

As a result of the project, the desired enhancement in the capacity of Bridge G-270 was achieved. This overall conclusion is based on results and extrapolations from laboratory tests, analysis, and in-situ tests.

REFERENCES

AASHTO *Standard Specifications for Highway Bridges* (1996), 16th Edition, 760 pp.

Al-Tayyib, A., and Khan, M. (1988), "*Corrosion Rate Measurements of Reinforcing Steel in Concrete by Electrochemical Techniques*", ACI Materials Journal, Vol. 85 No. 3, pp. 172-177.

Andrade, C., Castelo, V., Alonso, C., and Gonzales, J.A. (1986), "*The Determination of the Corrosion Rate of Steel Embedded in Concrete by the Polarization Resistance and AC Impedance Method*", Corrosion Effect of Stray Currents and the Techniques for Evaluating Corrosion of Rebars in Concrete, ASTM STP 906, pp. 43-63.

Berke, N.S., Hicks, M.C. (1990), "*Electrochemical Methods of Determining the Corrosivity of Steel in Concrete*", Corrosion Testing and Evaluation, ASTM STP 1000, pp. 425-440.

Berset, J.D. (1992), "*Strengthening of Reinforced Concrete Structures for Shear Using Composite Materials*," M.Sc. Thesis, MIT, Cambridge, Mass., 105 pp.

Broutman, L. J. (1974), *Fracture and Fatigue*, Academic Press, New York, NY, 465 pp.

Clear, K.C. (1990), "*Measuring Rate of Corrosion of Steel in Field Concrete Structures*", Transportation Research Record No. 1211, pp. 581-588.

Demers, C.E. (1998), "*Bending Fatigue Test of Prestressed Concrete Beams Reinforced with Carbon Fiber Sheets*", Construction and Building Materials, Vol. 12, No. 5, pp. 311-318.

Jones, D.A. (1996), *Principles and Prevention of Corrosion*, Prentice Hall, Englewood Cliffs, NJ, 572 pp.

Kaiser, H. (1989), "*Strengthening of Reinforced Concrete with Epoxy-Bonded Carbon-Fiber Plastics*," Ph.D. Thesis, ETH, Zurich, Switzerland, (in German).

L'Hermite, R.L, and Bresson, J. (1967), "*Beton Armé par Collage des Armatures*," RILEM Int. Symp., Resin in Building Construction, Part 2, Paris, pp. 175-203.

Mac Gregor, J. C. (1997), *Reinforced Concrete Mechanics and Design*, 3rd Edition, Prentice-Hall, Inc., Upper Saddle River, NJ, 939 pp.

Matsuoka, K., Kihira, H., Ito, S., and Murata, T. (1990), "*Corrosion Monitoring for Reinforcing Bars in Concrete*", Corrosion Rates of Steel in Concrete, ASTM STP 1065, pp. 103-117.

Mattock, A.H., Kriz, L.B., and Honegstad, E. (1961), "*Rectangular Concrete Stress Distribution in Ultimate Strength Design*", ACI Journal, Proceedings, Vol. 32, No. 8, pp. 875-928.

MBrace™ *Composite Strengthening System – Design Guide* (1998), Master Builders Technologies, Cleveland, Ohio, pp. 3.2-3.6.

Meier, U. (1987), "*Bridge Repair with High-Performance Composite Materials*," Material und Technik, Vol. 4, pp. 125-128 (in German).

Meier, U. and Kaiser, H.P. (1991), "*Strengthening of Structures with CFRP Laminates*", Proceedings: Advanced Composite Materials in Civil Engineering Structure, ASCE Specialty Conference, pp. 224-232.

Miller, B. (1999), "*Bond Between Carbon Fiber Reinforced Polymer Sheets and Concrete*", MSc. Thesis, Department of Civil Engineering, University of Missouri – Rolla, Rolla, MO, pp. 138.

Mitsubishi Chemical (1994), "*REPLARK: Carbon Fiber Prepreg for Retrofitting and Repair Method*," Manufacturer Publication, Tokyo, Japan, 18 pp.

Nanni, A., Ed. (1993), *Fiber-Reinforced-Plastic (FRP) Reinforcement for Concrete Structures: Properties and Applications*, Developments in Civil Engineering, Vol. 42, Elsevier, Amsterdam, The Netherlands, pp. 450.

Nanni, A. and Dolan, C.W., Eds. (1993), *"FRP Reinforcement for Concrete Structures*," Proc., ACI SP-138, American Concrete Institute, Detroit, MI, pp. 977.

Nanni, A. (1997), "*Carbon FRP Strengthening: New Technology Becomes Mainstream*", Concrete International: Design and Construction, Vol. 19, No. 6, pp. 19-23.

Nilson, A. H. (1997), *Design of Concrete Structures*, 12th Edition, McGraw-Hill, New York, NY, 780 pp.

Nishizaki, I., Sakamoto, H., Sasaki, I, and Abe M. (1997), "*Bending Fatigue Test of Prestressed Concrete Beams Reinforced with Carbon Fiber Sheets in Water Environment*", Non-metallic (FRP) Reinforcement for Concrete Structures, Proceedings of the Third International Symposium, T. Ueda Editor, Sapporo, Japan, Vol. 1, pp. 387-394.

Ritchie, P.A., Thomas, D.A., Lu, L.W. and Connely, G.M. (1991), *"External Reinforcement of Concrete Beams Using Fiber Reinforced Plastics*", ACI Structural Journal, Vol. 88, No. 4, pp. 490-500.

Roberts, T.M. and Haji-Kazemi, H. (1989), *"Theoretical Study of the Behavior of Reinforced Concrete Beams Strengthened by Externally Bonded Steel Plates*," Proc. Inst. Civ. Engrs, Part 2, 39-55.

Rostasy, F.S., and Budelman, E.H. (1992), *"Strengthening of RC and PC Structures with Bonded FRP Plates*, " Proceedings, Advanced Composite Materials in Bridges and Structures, K. Neale and P. Labossière Editors, Sherbrooke, Canada, pp. 253-263.

Saadatmanesh, H. and Ehsani, M. (1991), "*RC Beams Strengthened with GFRP Plates. II: Analysis and Parametric Study*", Journal of Structural Engineering, ASCE, Vol. 117 No. 11, pp. 3434-3455.

Shahawy, M., Beitelman, T. E. (1998), "*Fatigue Performance of RC Beams Strengthened with CFRP Laminates*", Proceedings: Durability of Fiber Reinforced Polymers (FRP) Composites for Constructions, University of Sherbrooke, Sherbrooke, Canada, pp. 169-178.

Sharif, A., Al-Sulaimani, G.J., Basunbul, I.A., Baluch, M.H. and Ghaleb, B.N. (1994), "*Strengthening of Initially Loaded Reinforced Concrete Beams Using FRP Plates*," ACI Structural Journal, Vol. 91, No. 2, pp. 160-168.

Shaw, B.A., Frankel, G.S., Murray, J., and Pickering, H.W. (1997), *Short Course on Corrosion: Fundamentals and Experimental Methods*, Penn State University Corrosion Center.

Small, Edgar P. (1998), *Condition of the Nation's Highway Bridges*, TR News, Transportation Research Board, No. 194, pp. 3-8.

Swamy, R.N., Jones, R. and Bloxham, J.W. (1987), *"Structural Behavior of Reinforced Concrete beams Strengthened by Epoxy-Bonded steel Plates*", The Structural Engineer, Vol. 65A, No. 2, pp. 59-68.

Todeschini, C., Bianchini, A., and Kesler, C. (1964), *"Behavior of Concrete Columns Reinforced with High Strength Steels*", ACI Journal, Proceedings, Vol. 61, No. 6, pp. 701-716.

Tonen (1994), *"FORCA Tow Sheet Technical Notes,"* Manufacturer Publication, Rev. 1.0, Tokyo, Japan, 55 pp.

Triantafillou, T.C. and Plevris, N. (1990), "*Flexural Behavior of Concrete Structures Strengthened with Epoxy-Bonded Fiber Reinforced Plastics*," Proceedings of the

International Seminar on Structural Repairs/Strengthening by the Plate Bonding Technique, University of Sheffield, Sheffield, England.

Wheat, H.G., Aliezer, Z. (1985), "*Some Electrochemical Aspects of Corrosion of Steel in Concrete*", Corrosion, Vol. 41, No. 11, pp. 640-645.

APPENDIX A

LOCATION OF BRIDGE G-270

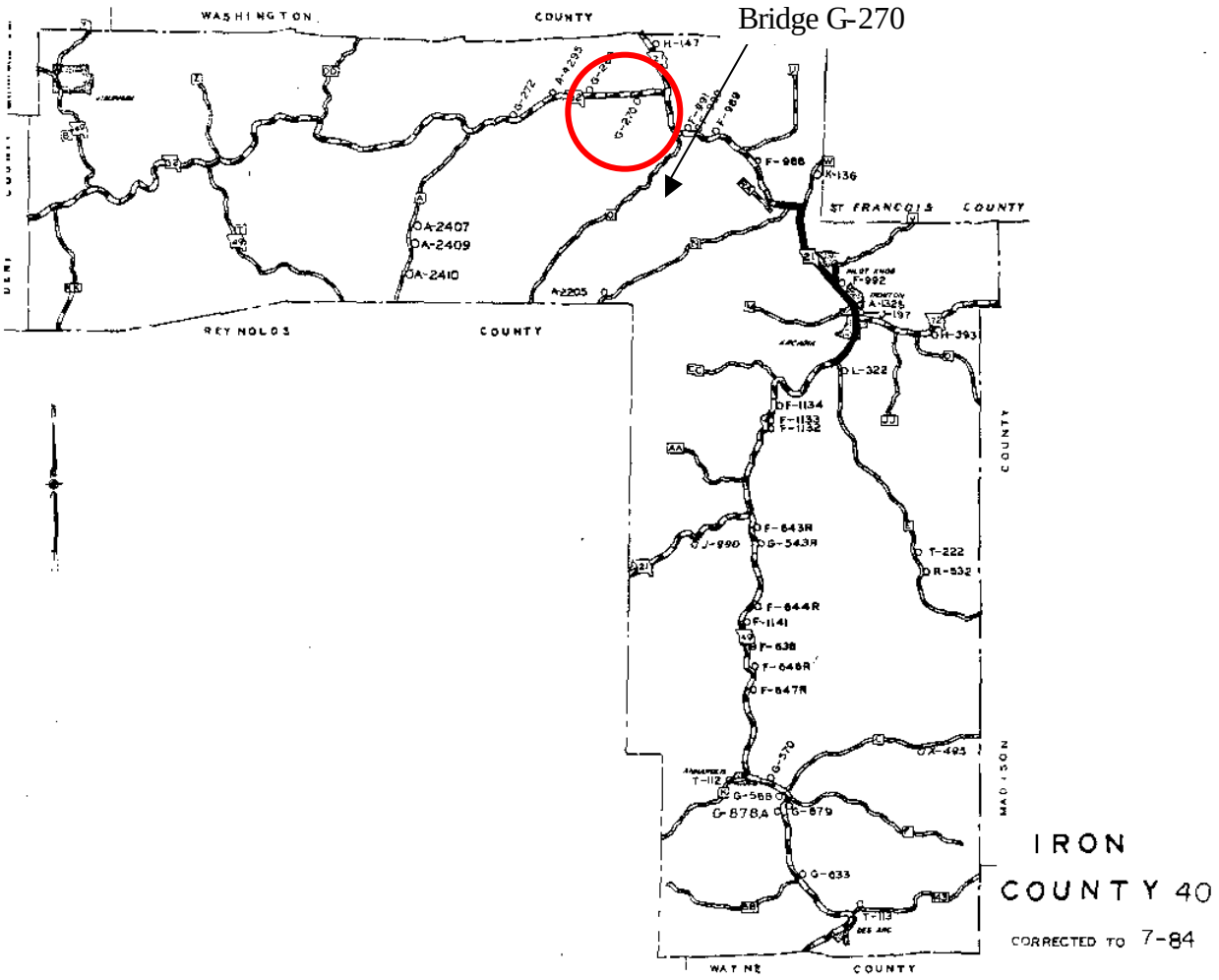

Figure A.1. Location of Bridge G-270

APPENDIX B

BRIDGE DRAWINGS

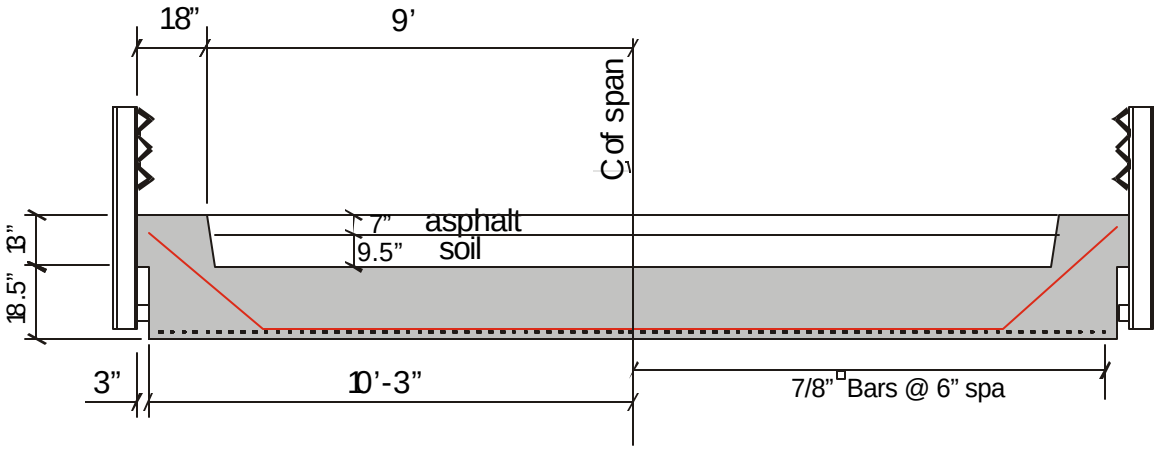

Note: 1 in. = 25.4 mm; 1 foot = 0.3048 m

Figure B.1. Typical Section Through Bridge Deck (Reconstructed)

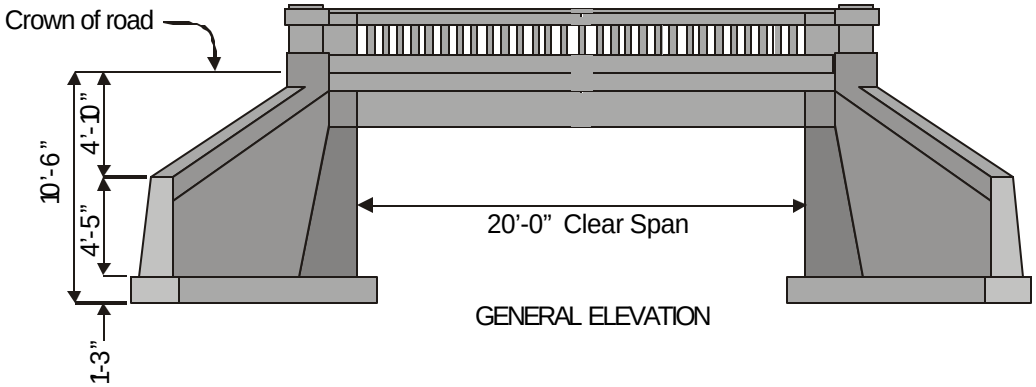

Note: 1 in. = 25.4 mm; 1 foot = 0.3048 m

Figure B.2. General Plan and Elevation (Reconstructed)

APPENDIX C

MATERIAL SPECIFICATIONS

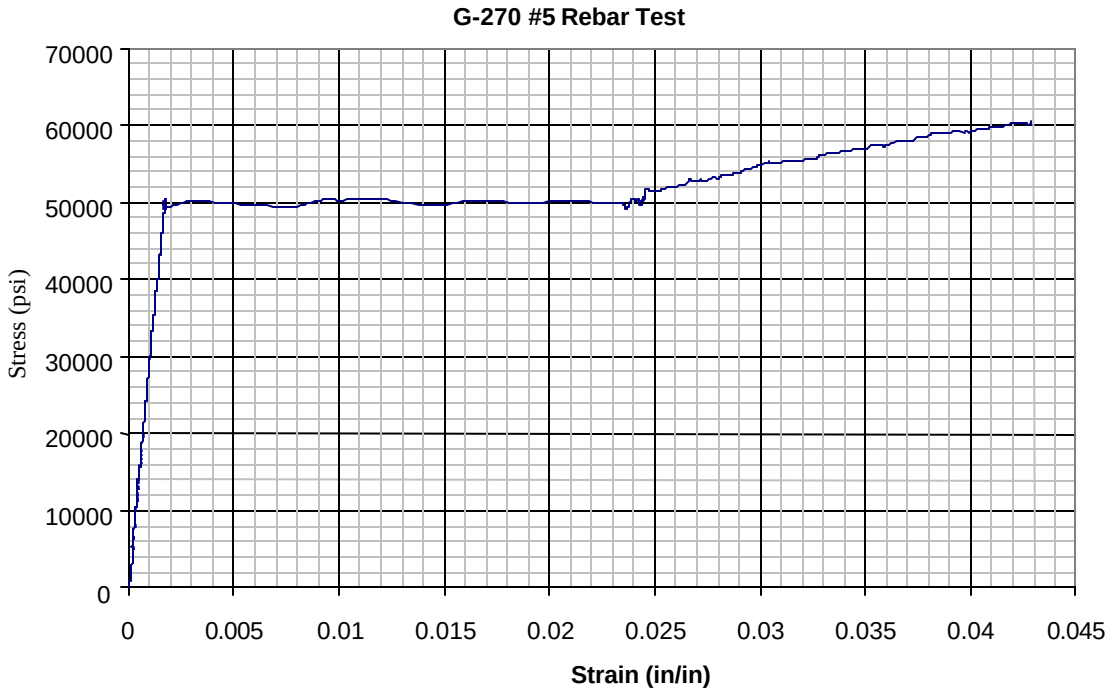

Figure C.1. Stress-strain Curve of Steel Rebar #5
Note: 1000 psi = 6.9 MPa

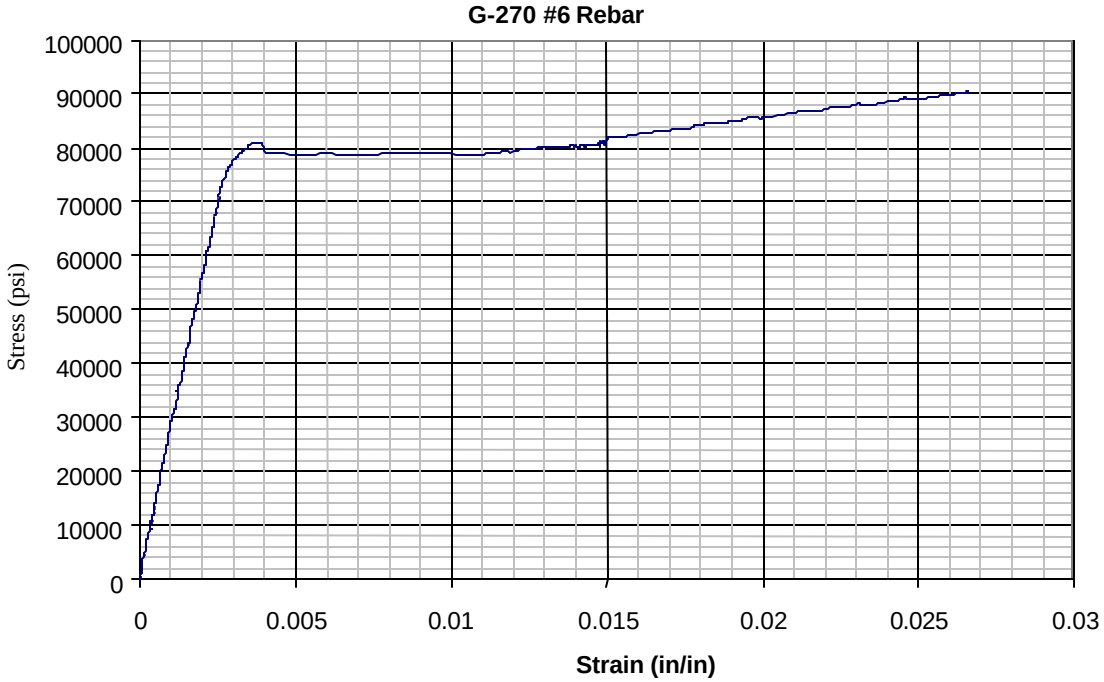

Figure C.2. Stress-strain Curve of Steel Rebar #6
Note: 1000 psi = 6.9 MPa

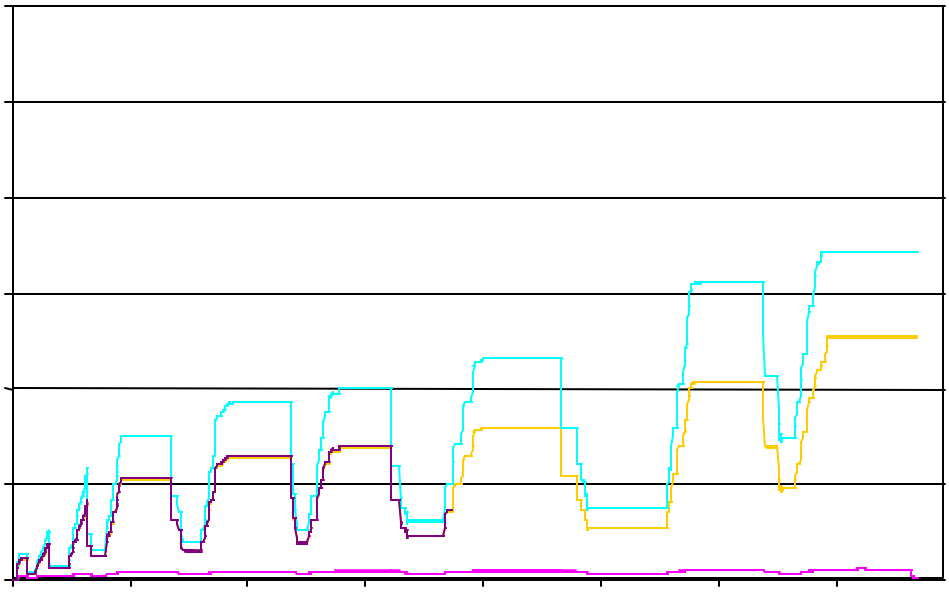

Figure C.3. Deflection-Time History for Beam Test #1 (Unstrengthened)
Note: 1 in = 25.4 mm; 1 lb = 4.45 N

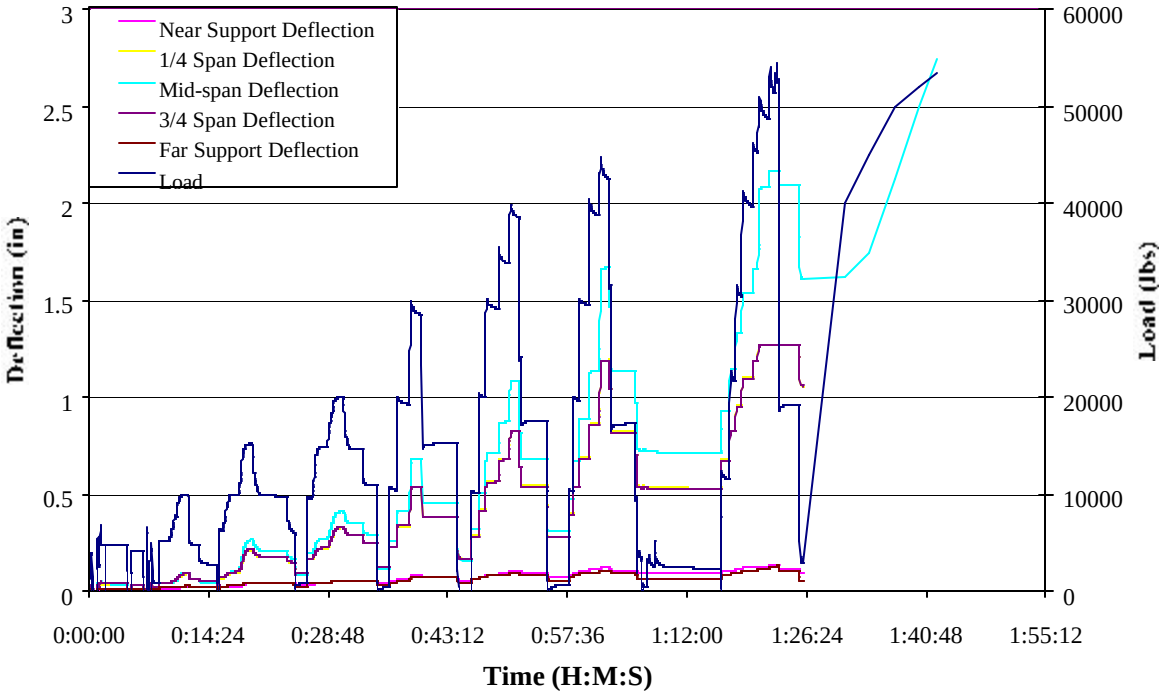

Figure C.4. Deflection-Time History for Beam Test #2 (Strengthened)
Note: 1 in = 25.4 mm; 1 lb = 4.45 N

APPENDIX D

BRIDGE RATING VEHICLES

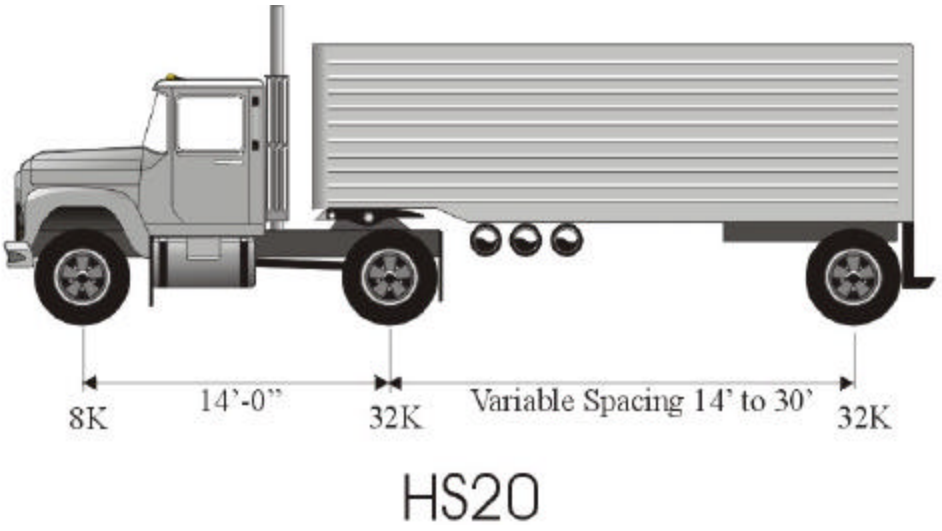

Figure D.1. Truck HS20

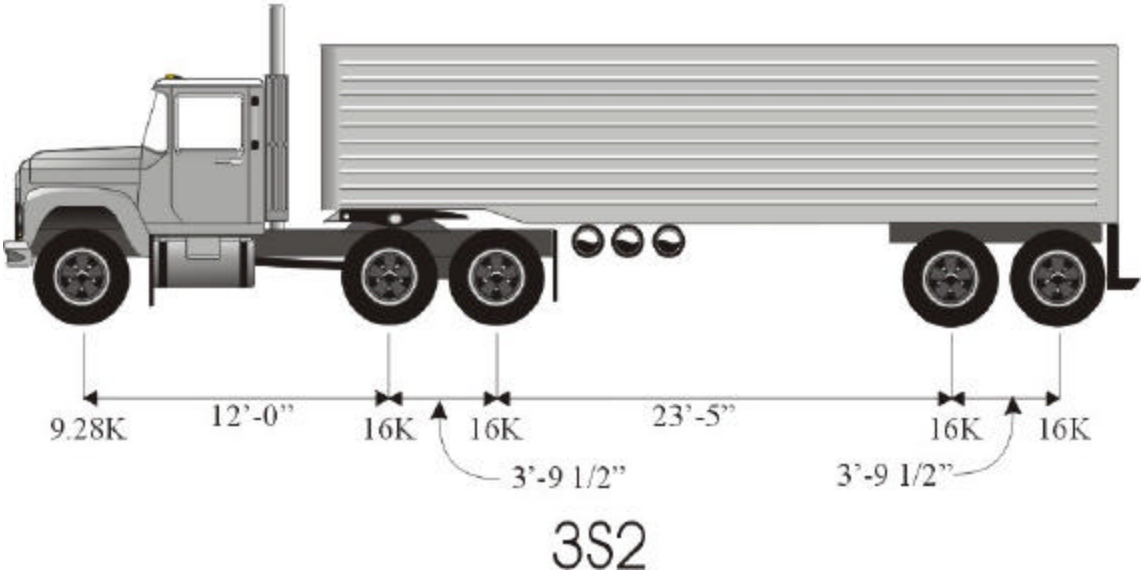

Figure D.2. Truck 3S2

Note: 1 ft = 12 in = 304.8 mm; 1 kip = 4.45 kN

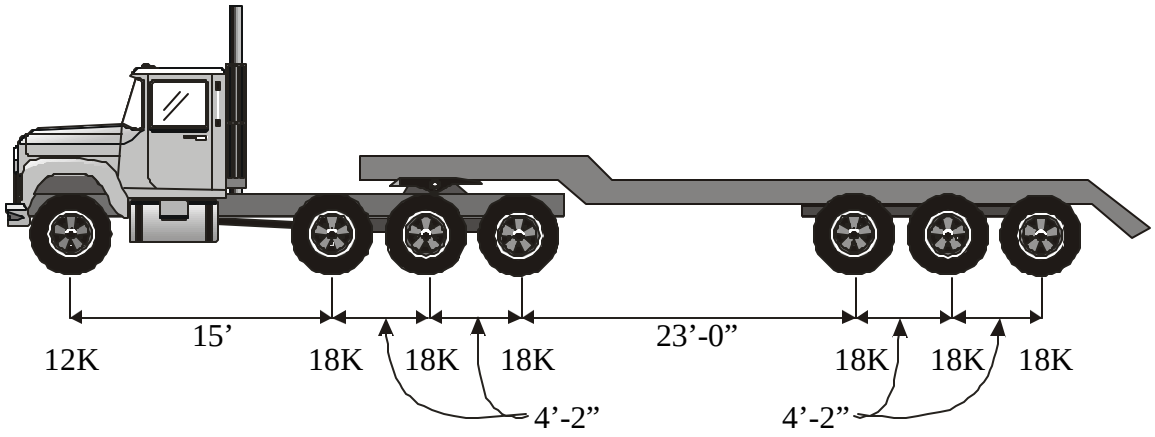

Figure D.3. Truck 4S3P

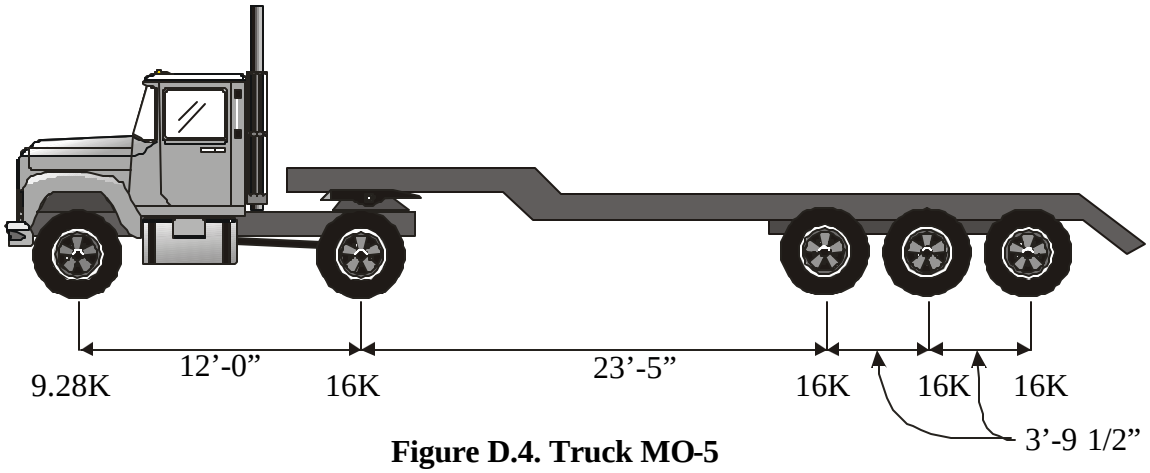

Figure D.4. Truck MO-5

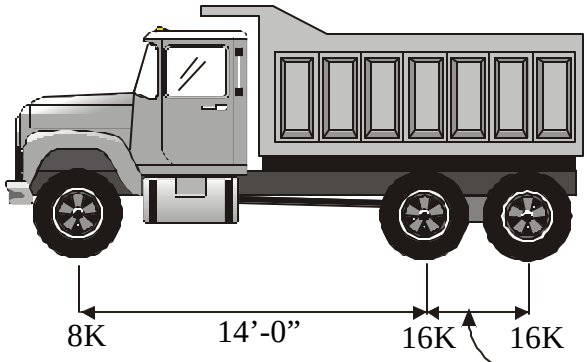

Figure D.5. Truck H20

Note: 1 ft = 12 in = 304.8 mm; 1 kip = 4.45 kN

APPENDIX E

AUTOMATED CALCULATIONS

CFRP Flexural Strengthening

Ultimate Strength Design with Service Load Check

Project: Iron County Bridge G-270

University of Missouri - Rolla

Geometry:

$h := 18.5$	Height of overall section under consideration
$b := 12$	Width of web
$L := 21.25 \cdot 12$	Length of span
$L1 := 21.25 \cdot 12$	Length of loaded span(s). For multiple spans, use the length of one bay for positive moment regions, two bays for negative moment regions. [2]

Concrete Properties:

$f'c := 2363$	Nominal concrete compressive strength
$\varepsilon cu := 0.003$	Ultimate strain level for concrete:

Mild Steel Properties:

$As := 1.53$	Area of mild tension steel (zero is acceptable) 2#7 square
$ds := 16.75$	Depth to the mild tension steel centroid
$fsy := 30000$	Yield strength of mild steel
$Es := 29000000$	Modulus of elasticity for mild steel

CFRP Properties:

$tf := 0.0065$	Thickness of one layer of CFRP
$ffu := 550000$	Ultimate strength of CFRP
$\varepsilon fu := 0.015$	Ultimate strain in the CFRP
$Ef := 33000000$	Modulus of elasticity for CFRP

Allowable Stresses:

$fcA := 0.45 \cdot f'c$	Allowable stress in concrete
$fsA := 0.80 \cdot fsy$	Allowable stress in mild steel
$ffA := 0.33 \cdot 0.95 \cdot 0.65 \cdot ffu$	Allowable stress in FRP

Preliminary Calculations

Preliminary computations for concrete material properties:

$Ec := 57000\cdot\sqrt{f'c}$ $\quad Ec = 2.771\cdot 10^{6}$ Modulus of elasticity for concrete

$\varepsilon co := \frac{1.71\cdot f'c}{Ec}$ $\quad \varepsilon co = 1.458\cdot 10^{-3}$ Peak value of strain corresponding to f'c [1]

Prelimiary computations for Gross Section Properties:

Cross sectional area:

$Ac := b\cdot h$

$Ac = 222$

Distance from the top fiber to the centroid:

$$ct := \frac{\left[\sqrt{\left[\frac{Es}{Ec}\cdot(As)\right]^2 + 2\cdot b\cdot\frac{Es}{Ec}\cdot As\cdot ds} - \frac{Es}{Ec}\cdot As\right]}{b} \qquad ct = 5.484$$

Distance from the bottom fiber to the centroid:

$cb := ds - ct$

$cb = 11.266$

Cracked moment of inertia:

$$Ic := \left(b\cdot\frac{ct^3}{12}\right) + b\cdot ct\cdot\left(\frac{ct}{2}\right)^2 + \frac{Es}{Ec}\cdot\left[As\cdot(ds - ct)^2\right]$$

$Ic = 2.692\cdot 10^{3}$

Effective width of concrete in compression:

$be := b$

$be = 12$

Preliminary computations for approximate existing strain conditions:

$\omega d := Ac\cdot\frac{150}{12^3}$ $\quad \omega d = 19.271$ Uniform self-weight:

$Md := (14.173 + \omega d)\cdot\frac{L^2}{8}$ $\quad Md = 2.718\cdot 10^{5}$ Approximate moment due to self-weight plus superimposed dead load.

$\varepsilon ob := \left[\frac{Md\cdot(h - ct)}{Ec\cdot Ic}\right]$ $\quad \varepsilon ob = 4.743\cdot 10^{-4}$ Unloaded State of Strain at bot fiber (Compression is positive)

FRP Strengthening Analysis Strain Compatibility Analysis

Function defining the strain in the CFRP at ultimate:

$$\varepsilon f(c) := \min\left(\left[\varepsilon cu\cdot\frac{h-c}{c} - \varepsilon ob \quad \varepsilon fu\right]\right)$$

Function defining the stress in the CFRP at ultimate:

$$ff(c) := \varepsilon f(c)\cdot Ef$$

Function defining the strain in the concrete at ultimate:

$$\varepsilon c(wf,c) := \left[if\left[wf>0, \min\left[\left[(\varepsilon f(c)+\varepsilon ob)\cdot\frac{c}{h-c} \quad \varepsilon cu\right]\right], \varepsilon cu\right]\right]$$

Function defining the stress distribution in the concrete [1]:

$$fc(wf,c,y) := \left[\frac{2\cdot(0.9\cdot f'c)\cdot\left(\frac{\varepsilon c(wf,c)\cdot y}{\varepsilon co\cdot c}\right)}{1+\left(\frac{\varepsilon c(wf,c)\cdot y}{\varepsilon co\cdot c}\right)^2}\right]$$

Function defining the strain in the mild tension steel at ultimate:

$$\varepsilon s(wf,c) := \varepsilon c(wf,c)\cdot\frac{ds-c}{c}$$

Function defining the stress in the mild tension steel at ultimate:

$$fs(wf,c) := if\left(\varepsilon s(wf,c)<\frac{fsy}{Es}, \varepsilon s(wf,c)\cdot Es, fsy\right)$$

Function defining the distance from the top of the section to the centroid of the concrete stress block:

$$yc(wf,c) := c - \frac{\int_0^c fc(wf,c,y)\cdot be\cdot y\,dy}{\int_0^c fc(wf,c,y)\cdot be\,dy}$$

Function defining the total compressive force contributed by the concrete:

$$Cc(wf,c) := \int_0^c fc(wf,c,y)\cdot be\,dy$$

$$FailureMechanism(wf,c) := if(wf>0, if(\varepsilon f(c)<\varepsilon fu, 1, 2), 1)$$

FRP Strengthening Design

$wf := 4$ The total width of FRP

$c := 0.15 \cdot ds$ Trial value of the neutral axis location

Horizontal Equilibrium to find the value of c:

Given $Cc(wf, c) - As \cdot fs(wf, c) - tf \cdot wf \cdot ff(c) = 0$

$c := Find(c)$

Rotational Equilibrium to find the resistive moment:

$Mn1 := (As \cdot fs(wf, c) \cdot (ds - yc(wf, c)))$

$Mn := Mn1 + tf \cdot wf \cdot ff(c) \cdot (h - yc(wf, c))$ $\frac{Mn}{12000} = 77.715$

Design Moment Capacity:

$\phi Mn := \frac{0.9 \cdot Mn}{12000}$ $\phi Mn = 69.944$ k-ft

Other quantities of interest:

$c = 2.862$ Actual depth to the neutral axis

$\varepsilon c(wf, c) = 2.832 \cdot 10^{-3}$ Maximum compressive strain level in the concrete at ultimate

$\varepsilon s(wf, c) = 0.014$ Strain level in the mild tension steel at ultimate (tension is positive)

$\varepsilon f(c) \cdot \frac{wf}{wf} = 0.015$ Strain level in the FRP at ultimate

$FailureMechanism(wf, c) = 2$ The governing mode of failure.
A FailureMechanism value of "1"corresponds to concrete crushing
A FailureMechanism value of "2" corresponds to FRP rupture

Check Serviceability

Service load moment

$Af := tf \cdot wf$ $Ms := 42 \cdot 12000$

$$kd := \frac{\left[\sqrt{\left[\frac{Es}{Ec}\cdot(As)+\frac{Ef}{Ec}\cdot Af\right]^2+2\cdot b\cdot\left(\frac{Es}{Ec}\cdot As\cdot ds+\frac{Ef}{Ec}\cdot Af\cdot h\right)}-\left(\frac{Es}{Ec}\cdot As+\frac{Ef}{Ec}\cdot Af\right)\right]}{b}$$

$kd = 5.532$

$$Sfs := \frac{\left[Ms+\varepsilon ob\cdot Af\cdot Ef\cdot\left(h-\frac{kd}{3}\right)\right]\cdot(ds-kd)\cdot(Es)}{\left[As\cdot Es\cdot\left(ds-\frac{kd}{3}\right)\cdot(ds-kd)+Af\cdot Ef\cdot\left(h-\frac{kd}{3}\right)\cdot(h-kd)\right]}$$

$Sfs = 21851$ Stress in mild steel at service

$$Sfc := Sfs\cdot\frac{kd\cdot Ec}{Es\cdot(ds-kd)}$$

$Sfc = 1030$ Maximum compressive stress in concrete at service

$$Sff := \left[Sfs\cdot\left(\frac{Ef}{Es}\right)\cdot\frac{(h-kd)}{(ds-kd)}\right]-\varepsilon ob\cdot Ef$$

$Sff = 13091$ Stress in FRP at service

Allowable Stress Check

The following values must all be greater than 1 for the section to meet allowable stress requirements:

$\frac{fcA}{Sfc} = 1.033$ Allowable stress check of concrete (0.45 f'c).

$\frac{fsA}{Sfs} = 1.098$ Allowable stress check of mild steel (0.80 fy).

$\frac{ffA}{Sff} = 8.562$ Allowable stress check of FRP (0.33)(0.65)(0.95)ffu).